Palaeogeography, Palaeoclimatology, Palaeoecology 689 (2026) 113668

Contents lists available at ScienceDirect

Palaeogeography, Palaeoclimatology, Palaeoecology

journal homepage: www.elsevier.com/locate/palaeo

Preservation of ephemeral microbial fabrics: late Messinian filamentous dendrolites from the Salento Peninsula (central Mediterranean)☆

Alessandro Vescogni [a,*], Adriano Guido [b]

[a] Dipartimento di Scienze Chimiche e Geologiche, University of Modena e Reggio Emilia, via Campi 103, 41125 Modena, Italy
[b] Dipartimento di Biologia, Ecologia e Scienze della Terra, University of Calabria, via Bucci, cubo 15b, 87036 Rende, Cosenza, Italy

ARTICLE INFO

Editor: L Angiolini

Keywords:
Late Messinian
Microbialite
Dendrolite
Central Mediterranean

ABSTRACT

During the late Messinian, the Mediterranean Sea underwent the "Messinian Salinity Crisis," a major event that shifted carbonate platforms from coral-dominated to microbialite-dominated systems. While upper Messinian microbial carbonates are well documented in the western Mediterranean, new findings from the central basin, particularly the Salento Peninsula, provide fresh insights into their diversity and evolution. This study focuses on enigmatic carbonate fabrics (ECF) from Salento, previously tentatively identified as dendrolites. A multidisciplinary approach, combining field observations, microscopic fabric analysis, and biogeochemical techniques (UV-epifluorescence and SEM/EDS), was applied to investigate their nature and palaeoenvironment. The Salento ECF consist of fan-like, lobate structures forming vertically elongated aggregates a few centimeters tall, with microstructures containing organic-derived micritic clots and filamentous remains consistent with cyanobacterial microfabrics. These features support their identification as filamentous dendrolites, comparable to modern analogues from Hamelin Pool, western Australia. Stratigraphic and facies analyses suggest they formed in a lagoonal environment, very shallow and with fluctuating conditions, influenced by unstable connections to the open sea. In particular, although strongly affected by reworking, the sedimentary textures and bioclastic assemblages associated with the dendrolites indicate a phase of warm, moderate-energy waters with near-normal marine chemistry. Unlike modern examples, which show minimal or no mineralization, the Messinian dendrolites display a well-cemented, originally aragonitic microfabric, potentially linked to elevated carbonate saturation or to specific microbial assemblages that facilitated their preservation. These findings represent the first fossil record of filamentous dendrolites and highlight the Messinian Mediterranean carbonate factories as a key archive for microbialite research.

1. Introduction

During the late Messinian, the Mediterranean experienced a profound environmental and biotic crisis, known as the 'Messinian Salinity Crisis', mainly triggered by the closure of the connections with the Atlantic Ocean (Roveri et al., 2014 and references therein). These deteriorating conditions had a significant impact on carbonate factories, which shifted from coral-dominated in the late Tortonian/early Messinian (Franseen et al., 1996), to microbialite-dominated in the late Messinian. Upper Messinian microbial carbonates are mainly known in the Mediterranean from the western part of the basin, with large and well-documented outcrops in southern Spain and north Africa (Esteban, 1979; Roep et al., 1979, 1998; Riding et al., 1991; Martin et al., 1993; Braga et al., 1995; Dabrio and Polo, 1995; Calvet et al., 1996; Feldmann and McKenzie, 1997; Krijgsman et al., 2001; Bourillot et al., 2020), but several examples have also been reported from the central sector (Pedley, 1978, 1979; Saint Martin and André, 1992; Saint Martin et al., 1996, 1997, 2023; Saint Martin, 2001; André et al., 2002; Moissette et al., 2002, 2010; Cornée et al., 2004; Vescogni et al., 2022, 2025). The abundance and diversity of these carbonates have led researchers to consider the late Messinian of the Mediterranean as a 'laboratory' for the study of microbialites, providing important insights into their characterization and evolution. For example, agglutinated stromatolite, which are locally common among present-day microbialites, were virtually unknown before the late Messinian (Riding, 2000) and their main fossil occurrences have been described from upper Messinian outcrops in

☆ This article is part of a Special issue entitled: 'Mediterranean Miocene' published in Palaeogeography, Palaeoclimatology, Palaeoecology.

* Corresponding author.
E-mail address: alessandro.vescogni@unimore.it (A. Vescogni).

https://doi.org/10.1016/j.palaeo.2026.113668
Received 13 October 2025; Received in revised form 5 February 2026; Accepted 21 February 2026
Available online 24 February 2026

Southern Spain (Riding et al., 1991; Martin et al., 1993; Braga et al., 1995). Similarly, upper Messinian carbonates from the Salento Peninsula (central Mediterranean) contain micro-laminated dendrolites and thrombolites with spheroidal microstructures that have not been previously documented elsewhere in the Cenozoic (Vescogni et al., 2025).

In this paper we focus on upper Messinian enigmatic carbonate fabrics (hereinafter referred to as ECF) coming from the same Salento outcrop described in Vescogni et al. (2025) (Fig. 1A). In a preliminary study on the upper Messinian carbonates of this area, these were tentatively compared with dendrolites (Vescogni et al., 2022), *i.e.* centimetric, branched, non-laminated growth-forms related to microbial calcification (Riding, 1988, 1991, 2000). Here we use a multidisciplinary approach to describe them, including: a) macroscopic field observations of the geometric, sedimentary, and palaeontological features of the stratigraphic interval containing the ECF and of the adjacent facies belonging to the same depositional system; b) microscopic characterization of ECF at centimeters to sub-millimeters scales; and c) biogeochemical analyses, including UV-Epifluorescence observation of small slabs and uncovered thin sections, and SEM/EDS analyses of unpolished fragments and gently etched thin sections. Finally, we compare these Salento examples with fossil and present-day dendrolites. This comparison integrates data from experimental analyses, providing further insights into the origin of the Salento ECF, the potential microbial consortia responsible for their growth, and their depositional and palaeoenvironmental conditions.

2. Geological setting

The Salento Peninsula (Fig. 1A) is located within the southernmost emergent part of the Apulia Platform, a major element within the complex structural framework of the Mediterranean basin. As a northern fragment of the African Plate, during the Mesozoic the Apulia Platform was positioned along the southern margin of the Tethyan Ocean and since the Triassic has hosted the deposition of shallow-water carbonates. From the Late Cretaceous to the Cenozoic, it was involved in the complex sequence of events associated with the closure of the Tethys Ocean, which eventually led to its collision with the European Plate. As a result, the area corresponding to the present-day Salento Peninsula experienced further shallowing, leading to the formation of an isolated, partially emergent platform. Along the margins of this plateau, several carbonate formations were deposited, interrupted by significant hiatuses due to major episodes of erosion. These carbonate systems mainly consist of clinostratified bioclastic deposits and coral reefs, ranging in age from the Late Cretaceous to the Late Pleistocene. These units can be traced along the south-eastern coast of the Salento Peninsula from Otranto to the Leuca Cape (Fig. 1A). Detailed information on the structural and stratigraphic setting of the southern Salento can be found in Bosellini et al. (1999), Ricchetti and Ciaranfi (2013) and Milli et al. (2024).

In the Leuca surroundings the succession starts with the Altamura Limestone Formation, here represented mainly by Campanian/Maastrichtian peritidal cycles (Bosellini et al., 1999), followed by the Castro Limestone Formation, a lower Chattian coral reef system (Bosellini et al., 2021 and references therein), and by the *Aturia* Level, a thin Serravallian/Tortonian phosphatic hardground (Vescogni et al., 2018 and references therein) (Fig. 1B, C). The overlying Messinian limestones exhibit a complex configuration, influenced by the presence of various depositional environments and by changes in conditions over time (Bosellini et al., 2001, 2002; Bossio et al., 2002; Bosellini, 2006; Brachert et al., 2007; Vescogni et al., 2008a, 2011; Braga et al., 2009). Along the shelf margin the Messinian carbonates belong to the Novaglie Formation and display the superimposition of three depositional sequences (Fig. 1B, C). The first two (NF1 and NF2) consist of lower Messinian *Porites* reef margins with associated slope systems, respectively up to 120 m and 20

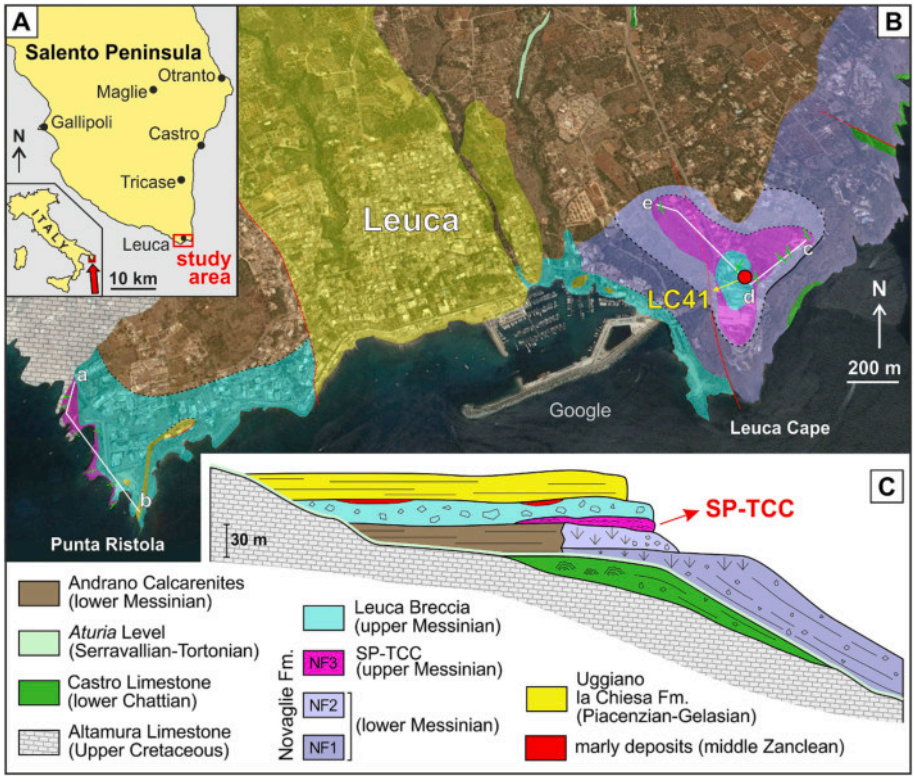

Fig. 1. A) Schematic map of the Salento Peninsula with the location of the study area. B) Geological map of the study area showing the position of the stratigraphic section (LC41) and the trace of the three transects depicting the SP-TCC architecture (a-b, c-d, d-e) reported in Fig. 2 (modified from Vescogni et al., 2022). C) Stratigraphic setting of the study area; the arrow highlights the stratigraphic unit considered in this study, referred to as SP-TCC (Salento Peninsula Terminal Carbonate Complex).

m in thickness. Both these sequences pass landward into a wide belt of oolitic and bioclastic sediments assigned to the Andrano Calcarenites Formation. Overlying the NF2 the third Novaglie Formation sequence (NF3) is a 12 m thick unit of oolitic calcirudites/calcarenites with microbialites, scattered *Porites* colonizations and small vermetid/serpulid bioherms. The NF3 is the stratigraphic interval considered in the present study. It has been recently dated to the late Messinian (Vescogni et al., 2022). Based on the close similarity in age and carbonate facies, it has been compared to the Terminal Carbonate Complex of the western Mediterranean, and thus named the Salento Peninsula Terminal Carbonate Complex (SP-TCC) (see discussion in Vescogni et al., 2022).

The SP-TCC is overlain by the upper Messinian Leuca Breccia Formation, consisting of breccia deposits about 12 m thick, derived from erosion of the underlying Messinian carbonates. The Leuca Breccia is followed by thin, scattered outcrops of middle Zanclean marls and by the Uggiano la Chiesa Formation, a Piacentian-Gelasian calcarenite and breccia succession up to several tens of meters in thickness (Bosellini et al., 1999).

3. SP-TCC stratigraphy and carbonate facies

A preliminary characterization of the SP-TCC was presented in Vescogni et al. (2022), including stratigraphic architecture, age determination and an analysis of the carbonate facies. The SP-TCC crops out at both sides of the Leuca harbor, and at the two locations, Punta Ristola to the west and Leuca Cape to the east (Fig. 1B), it exhibits substantially different facies associations. In Punta Ristola, the SP-TCC rests on coral breccia deposits of the NF2 or directly overlies the Cretaceous. It is up to 12 m thick and clearly displays a subdivision into three higher-frequency depositional cycles (Fig. 2A). Here, the succession consists mainly of oolitic/bioclastic packstones and grainstones, also associated with *Porites* colonizations and some thin horizons of laminated stromatolite. A sharp erosion surface marks the boundary with the overlaying Leuca Breccia Formation.

At the Leuca Cape the SP-TCC is up to six meters thick (Fig. 2B, C) and the majority of the succession consists primarily of microbial carbonates, which exhibit a wide range of arrangements and textures (Vescogni et al., 2022). In particular, the SP-TCC rests on top of NF2 slope deposits and starts with decimetric crusts and small mounds of coarse laminated stromatolite. This facies is followed by bioclastic grainstone, often cemented by peloidal micrite of microbial origin. Enclosed within these latter deposits two additional distinct facies have been identified: small, decimeter-thick lenticular serpulid/coralline algae bioherms, and a larger build-up composed of coalescent microlaminated dendrolites and thrombolites, recently described in Vescogni et al. (2025). The succession continues with several decimeters of oolitic grainstone, which is truncated by a sharp erosional surface. This allows for the correlation of this basal SP-TCC interval with the first depositional cycle at Punta Ristola.

The overlying upper portion of the SP-TCC at Leuca Cape (Fig. 2C) is the depositional system considered in this study. It is approximately 1.5 m thick and the description of the related facies and their stratigraphic relationships, briefly outlined in Vescogni et al. (2022), is discussed in greater detail later in the text. The reduced thickness of this interval, together with the presence of pronounced and sometimes overlapping erosion surfaces, makes it difficult to precisely correlate it with either the second or third depositional SP-TCC cycle observed along the western side of the Leuca Gulf. As in Punta Ristola, a major erosion

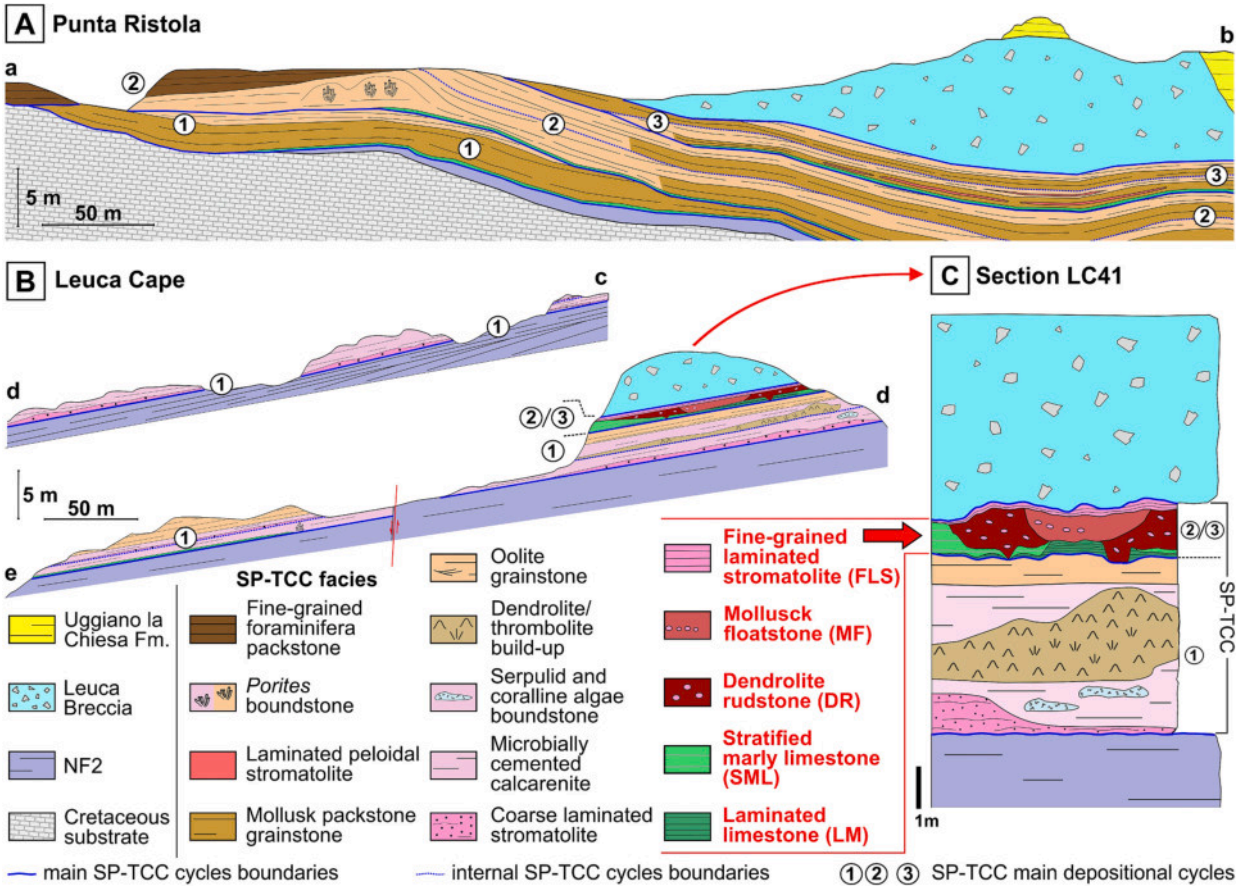

Fig. 2. SP-TCC stratigraphic settings and depositional facies: A) Punta Ristola (transect a-b). B) Leuca Cape (transects c-d, d-e). C) Stratigraphic section of the studied outcrop (LC41); the red arrow indicates the stratigraphic interval considered in this study, depositional facies related to this interval are shown in red. Modified from Vescogni et al. (2022). (For interpretation of the references to colour in this figure legend, the reader is referred to the web version of this article.)

surface at the top of the SP-TCC marks the upper boundary with the Leuca Breccia Formation.

4. Materials and methods

4.1. Stratigraphy and facies analysis

The depositional system considered in this study is located at Leuca Cape, along the section LC41, a vertical outcrop exposed by the roadcut just north of the Leuca lighthouse (39°47′51.49“N / 18°22’10.89”E) (Figs. 1B, 2C). Field observations enabled detailed characterization of the different facies, including their geometries, stratigraphic relationships, sedimentary features, and fossil content at the macroscopic scale. These data have been integrated with microfacies analyses: from a total of 49 samples, 64 thin sections (4.5 × 6 cm) were prepared to identify carbonate grains and textures. Microfacies observations were performed using a Leitz Orthoplan optical microscope at different magnifications (16×, 25×, 40×, 63×, 100×). Rock textures were described according to the classifications of Dunham (1962) and Embry and Klovan (1971).

4.2. ECF characterization

4.2.1. ECF structure

ECF were described at different scales, considering both their mesofabric (centimeter to millimeter scale), which includes size, shape and growth-form, and their microfabric (millimeter to sub-millimeter scale), with a focus on their internal structures. Both descriptions, as well as the relationships between ECF and the associated sediments, were based on microscopic observations of the same thin sections used for microfacies characterization. The description of ECF and their related aggregates follows the terminology of Shapiro and Wilmeth (2020) used for dendrolites, in which each growth-form, termed a “dendroid”, is differentiated into a central stem, referred to as the “trunk” from which several small “branches” of various shapes and sizes extend laterally and upward (Fig. 8 in Shapiro and Wilmeth, 2020).

4.2.2. UV-epifluorescence

UV-epifluorescence observation enables the detection and spatial distribution of organic compounds within the microfacies. This technique is particularly suitable in distinguishing, in combination with morphological features, mineral precipitates of biogenic origin from those formed through abiotic processes (*e.g.*, Neuweiler et al., 2000, 2003, 2023; Russo et al., 1997; Guido et al., 2022a, 2024; Cipriani et al., 2024). Small slabs and uncovered thin sections prepared for microfabric analysis were employed to assess the presence of organically activated luminescence. Fluorescence was induced using incident light emitted by a high-pressure mercury vapour lamp mounted on a Zeiss Axioplan Imaging II microscope. The system was equipped with high-performance wide bandpass filter sets to discriminate fluorescence emission based on wavelength. Specifically, a 436/10 nm band-pass excitation filter combined with a 470 nm long-pass emission filter (filter set no. 488006) was used to detect green fluorescence, while a 450–490 nm band-pass excitation filter paired with a 515 nm long-pass emission filter (filter set no. 488009) was employed to detect yellow fluorescence.

4.2.3. SEM-EDS

Scanning Electron Microscopy (SEM) coupled with Energy Dispersive X-ray Spectroscopy (EDS) allowed the investigation of morphology, size, and composition of the carbonate components within ECF and surrounding matrices. Selected samples were carbon-coated to ensure optimal conductivity and were analyzed using an Ultra High Resolution SEM (ZEISS CrossBeam 350). In particular, freshly fractured surfaces were used to allow better observation of crystal morphology and size. Imaging was conducted under the following operating conditions: resolution of 123 eV, accelerating voltage of 10 keV, probe current of 100 pA, and a working distance of 11 mm.

Elemental analyses were performed using EDS under the following parameters: accelerating voltage of 15 keV, probe current of 10 nA, working distance of 12 mm, take-off angle of 40°, and a live acquisition time of 30 s. These analytical conditions were optimized to allow accurate identification of the elemental composition at the microscale.

5. Results

5.1. Stratigraphy and facies analysis

The stratigraphic interval under consideration crops out laterally over approximately 42 m, with a variable thickness reaching a maximum of 1.5 m. Despite the limited size, these deposits exhibit a complex architecture (Fig. 3), comprising five distinct depositional facies. Each of these units is bounded at both its base and top by pronounced and irregular erosional surfaces, which contribute to their highly variable thicknesses. The topmost fine-grained laminated stromatolite is an exception, as its lower contact surface exhibits no clear evidence of erosion. These facies are described below in stratigraphic order:

- Laminated limestone (LM – 0/50 cm in thickness): slightly marly limestone with fine, planar to locally wavy lamination, including discontinuous dark laminae possibly related to organic matter concentrations (Fig. 4A). This micro-laminated mudstone contains very rare bioclasts, primarily fragments of small benthic foraminifera of uncertain attribution, and only rarely is disrupted by traces of bioturbation (Fig. 4B).
- Stratified marly limestone (SML – 0/60 cm in thickness): marly limestone with planar-parallel layers ranging in thickness from less than 1 cm to 5 cm (Fig. 4C). Microfacies analysis reveals a predominant micro-laminated mudstone, showing the alternation of thin layers of compact/peloidal micrite, sometimes with small concentrations of pellets, and micritic laminae with alignments of fenestrae (Fig. 4D). The latter display an irregular to horizontally elongated shape, vary in size and abundance among different laminae, and may be associated with small gastropod molds. Other types of grains are rare, represented mainly by miliolids, small rotaliids and small intraclasts made of pellets. Although very rare, it is worth noting the presence of ECF, preserved as isolated fragments and, in one instance, arranged in a branched growth form. The marly limestone strata may display evidence of bioturbation, with the disruption of the laminated texture.
- Dendrolite rudstone (DR – 25/140 cm in thickness): this facies is hosted within a very irregular depression carved into the sedimentary units described above (Fig. 3B). It is a rudstone with a packstone matrix and displays a massive appearance, formed by the accumulation of sub-spherical to irregular nodules up to several centimeters in size (Fig. 4E, F) associated with abundant oyster fragments. No distinct sedimentary structures or spatial organization have been observed, except for a denser concentration of nodules in the southeastern portion of the outcrop. Near the basal and lateral contacts with SML the nodules are frequently associated with centimeter-sized clasts derived from the erosion of the underlying marly limestone. Microfacies analysis of the nodules reveals two types of textures.

Type 1: packstone rich in ECF (Fig. 4G), preserved mainly as millimeter-sized fragments, and more rarely as larger, branched aggregates These remains partially preserve their microfabric and are described in detail in chapter 5.2. Other clasts are less abundant and consist of gastropod molds, oyster fragments, ostracods, echinoids, and small benthic foraminifers (mainly miliolids, some species of *Elphidium, Ammonia*, rare *Gypsina* and very small rotaliids). All these grains are embedded in a compact micrite, which may form denser coatings around some of the fragments.

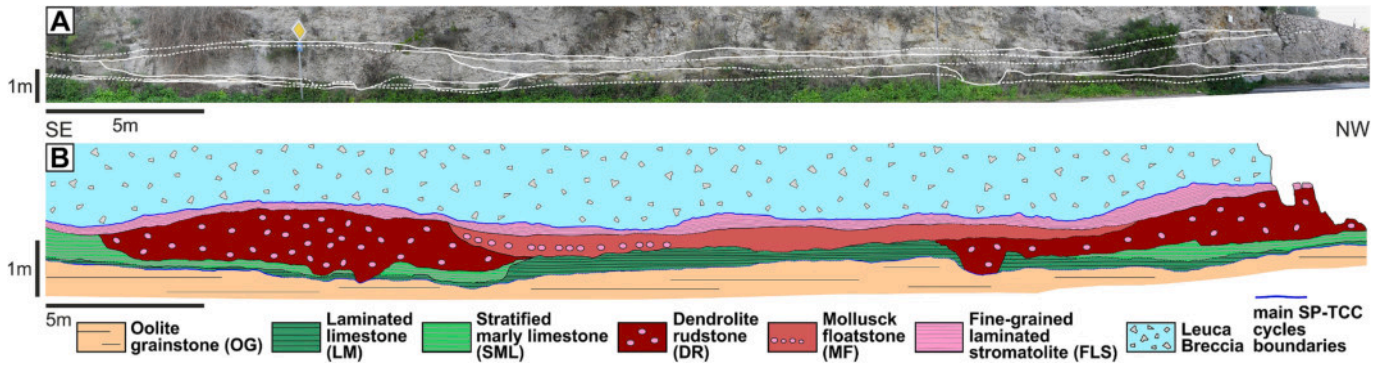

Fig. 3. A) Roadcut exposing the stratigraphic interval investigated in this study (upper portion of the LC41 section); continuous white lines denote the boundaries of depositional facies, whereas dashed lines are employed where such boundaries are uncertain. B) Schematic representation of the same interval illustrating the different depositional facies; note that the vertical scale is amplified to emphasize the geometric relationships.

Type 2: packstone/grainstone containing almost exclusively ECF (Fig. 4H), mainly preserved as recrystallized fragments, with only rare traces of the original microfabric. No branched aggregates have been observed in this case. These fragments frequently display very thin micro-laminated, ooid-like coatings and a micritic, sometimes peloidal, heavily recrystallized matrix (Fig. 4H, I).

These two textures do not show distinct spatial distribution and are closely associated, even within the same nodule. There is also a strong similarity between the sediment composing the nodules and the one surrounding them. Although macroscopically it appears more compact than the nodules (Fig. 4F), the rudstone matrix is actually composed of the same two packstones described above, once again intimately associated without precise spatial distribution.

- Mollusk floatstone (MF – up to 50 cm in thickness): this facies is hosted within an erosive depression incised into the DR and LM facies. It consists of a massive, slightly marly limestone containing abundant oyster and pectinid fragments (Fig. 5A). The floatstone matrix is fine-grained packstone that passes into wackestone and mudstone toward the top of the facies. These textures contain fragments of bivalves, gastropods, echinoderms, sparse small benthic foraminifera (small rotaliids, some species of *Elphidium, Gypsina*, miliolids) and ostracods (Fig. 5B). A rudstone horizon crosses the MF approximately halfway through its thickness (Fig. 5A), starting at the southwestern boundary with the DR and extending several meters toward the northwest. It is composed of coarse, isooriented bivalves and DR nodules. The occurrence of ECF appears to be very rare and limited to the DR nodules within this latter rudstone.
- Fine-grained laminated stromatolite (FLS - 20/60 cm in thickness): this last unit rests conformably on SML, DR and MF, with a generally sharp contact, though occasionally appearing more gradational. FLS consists of the superimposition of millimeter- to centimeter-thick undulated carbonate layers of different type (Fig. 5C): a) Mudstone layers with dense, sub-horizontal alignments of fenestrae, ranging from elongated to irregular in shape (Fig. 5D), sometime alternated with very thin laminae of calcite crystals. b) Packstone/wackestone layers containing gastropod molds, pellets, small benthic foraminifera (mainly miliolids), rare echinoderm and serpulid remains (Fig. 5E). c) Thin, undulose horizons of compact, micro-laminated mudstone (Fig. 5F) with sparse pellets, rarely showing traces of bioturbation.

5.2. ECF structure

ECF have been found mainly within the DR facies and are primarily preserved as fragments (Fig. 4G, H), although some of them appear to retain part or most of their original shape and fabric. In this latter case, they exhibit fan-like structures with a more or less jagged, lobate outline, ranging in size from 2 mm to over 1 cm (Fig. 6A-C). They also exhibit a variable height/width ratio, from relatively flattened (Fig. 6A) to more elongated (Fig. 6C). In a few cases, ECF has been found grouped into aggregates, allowing identification as basic elements forming more complex structures. On these occasions, the ECF described so far resemble branches, vertically or laterally oriented, tightly packed and grafted onto one another, forming elliptical, vertically elongated structures (Fig. 6D, E). These growth-forms can reach a maximum height of 3 cm and a width of 1 cm. A section cut perpendicular to the main axis reveals how, within these aggregates, ECF radiate outward from a more compact central area, forming irregular ramifications (Fig. 7A). In a single case a more complex arrangement was also observed, in which the ECF form a larger, mushroom-like structure approximately 4.5 cm high and 6 cm wide, with a basal trunk that broadens upward into a fan-shaped morphology (Fig. 7B). This structure is coated with thick, irregular encrustations of very dense micrite, often aphanitic and occasionally exhibiting a peloidal texture. ECF are engulfed in the type 1 bioclastic packstone described above, with a dark micritic matrix containing mollusk remains, ostracods, echinoderm fragments, and small benthic foraminifera (Fig. 6F).

ECF are usually heavily recrystallized, but in many cases, details of their internal microfabric can still be observed. These mainly consist of filaments, associated with small micrite clots. Filaments are several microns in diameter and may exhibit either long, straight forms (Fig. 6C) or more sinuous development (Fig. 7D), sometimes forming ramifications (Fig.7E). In some cases, filaments intertwine, forming tangles of various sizes (Fig. 7F). The ECF microfabric may contain rare, small bioclastic fragments, such as miliolids and small rotaliids (Fig.7C).

5.3. UV-epifluorescence

Under UV epifluorescence, the filaments and micritic clots forming the ECF microstructures display bright fluorescence, typically in the yellow-green spectrum (Fig. 8A-E). These fluorescent features are distributed throughout the internal portions of the ECF and are clearly visible at magnifications ranging from 50× to 200×. Fluorescent filaments are generally 20–30 μm in diameter and range from a few tens to several hundred micrometers in length. The walls of the filaments are often not discernible due to their micritized nature; however, by superimposing transmitted light with UV-excitation at varying light intensities (Fig. 9A, C, E), it is sometimes possible to enhance their intense epifluorescence, thereby revealing their extremely fine structure (<1 μm). This approach also improves the characterization of the areal distribution of organic compounds, which are predominantly concentrated in the cores of the peloids forming the micrite clots (Fig. 9B, D, F), which are irregular in shape and range in size from 20 to 100 μm.

A faint but consistent fluorescence was detected in the dark micrite of the type 1 packstone surrounding the ECF structures. This

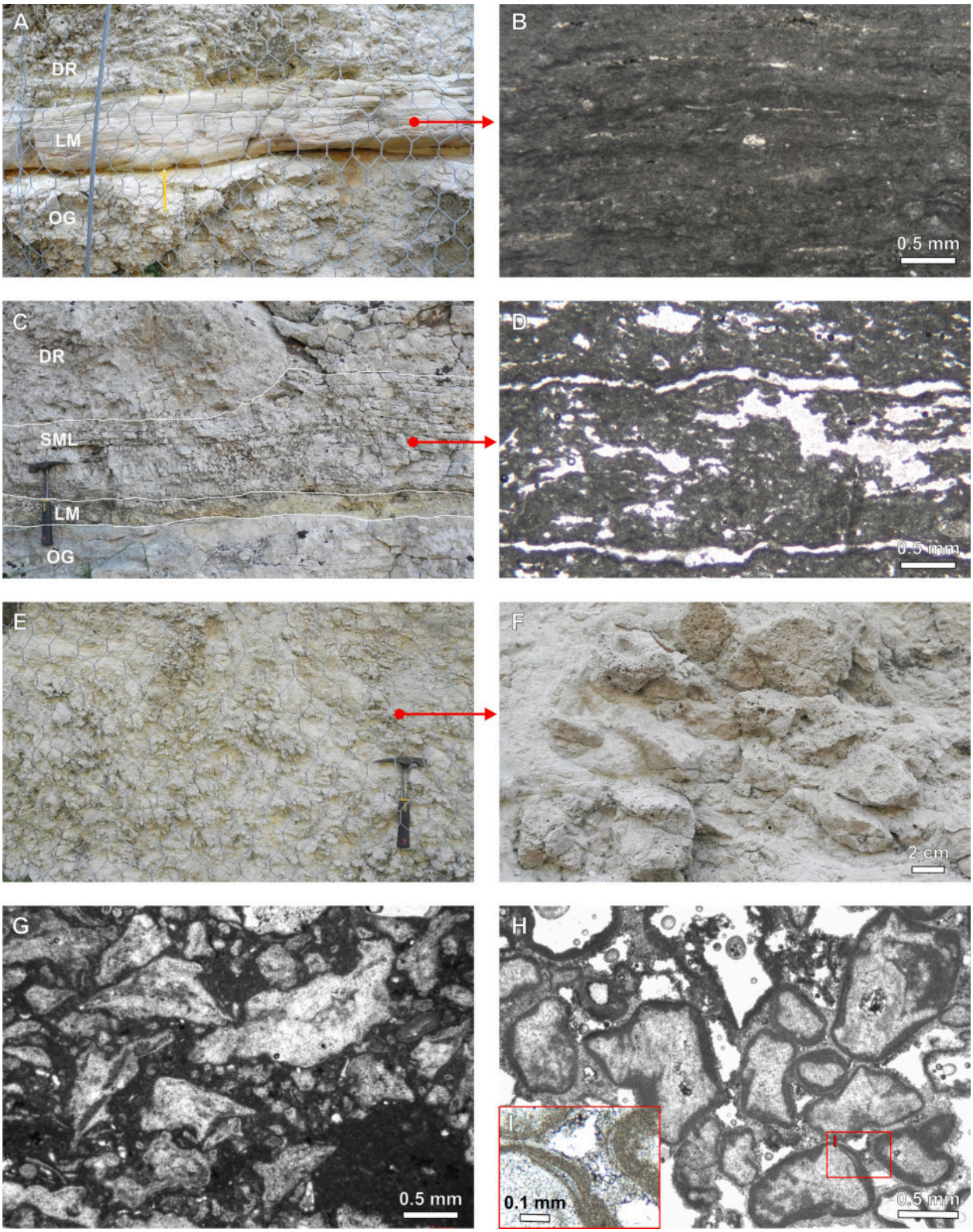

Fig. 4. A) Outcrop view of the laminated limestone facies (LM), resting on oolitic grainstone deposits (OG) and overlain by the dendrolite rudstone facies (DR). B) Thin section showing the LM micro-laminated texture; note the discontinuous darker laminae possibly related to concentrations of organic matter. C) Outcrop view of the stratified marly limestone (SML), with OG and LM at the base and DR facies at the top. D) Thin section of SML showing a micro-laminated mudstone texture with abundant fenestrae. E) Outcrop view of the DR facies, highlighting its nodular appearance. F) Outcrop close-up of the DR facies, detailing the nodules and surrounding matrix. G) Thin section of the DR facies type 1 packstone, showing ECF fragments embedded in dense, dark micrite. H) Thin section of type 2 packstone/grainstone from the DR facies, showing ECF fragments with ooid-like coatings and a heavy recrystallized micritic matrix. I) Detail of H showing the micro-laminated, ooid-like coatings on the ECF fragments.

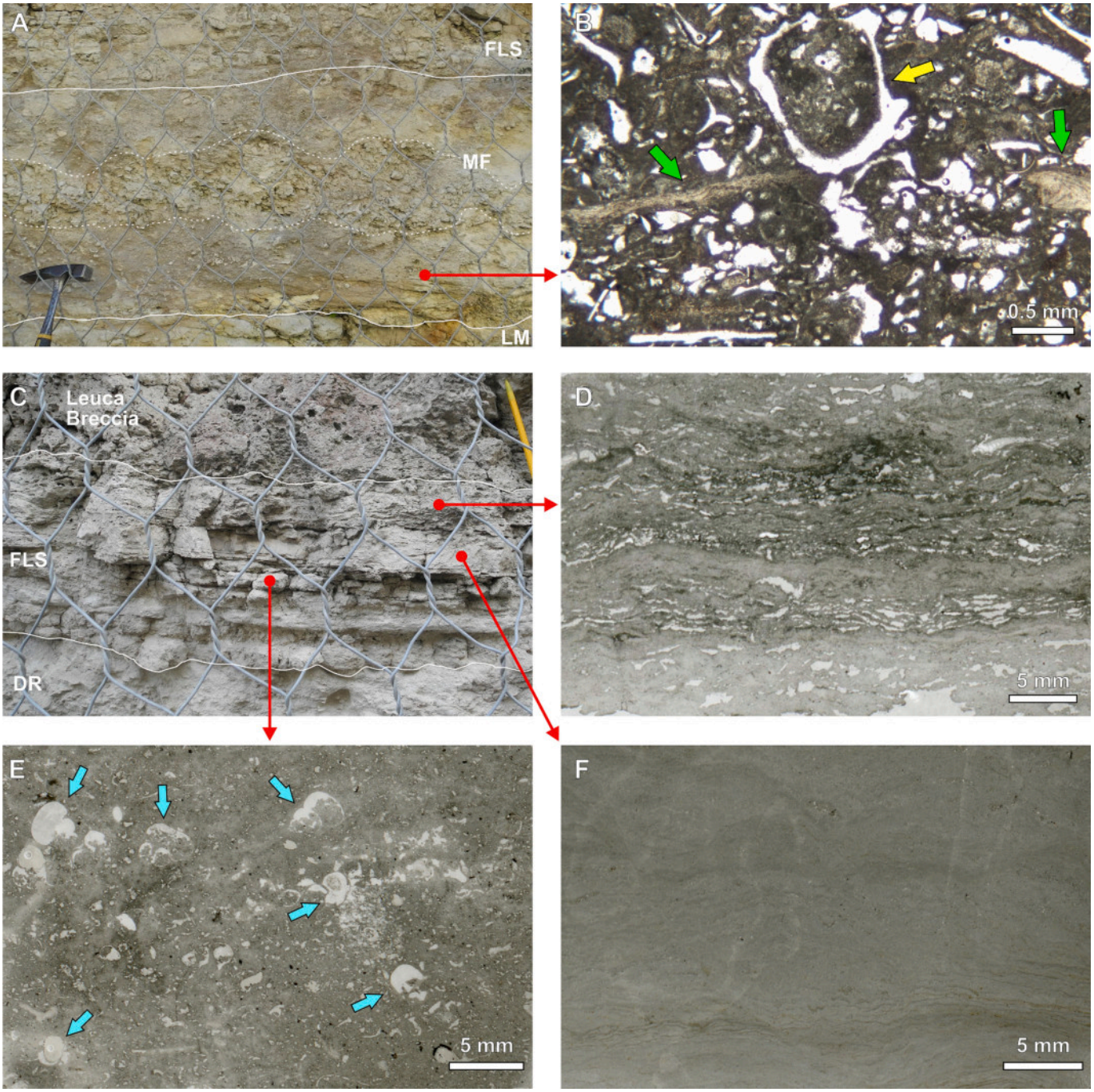

Fig. 5. A) Outcrop view of the mollusk floatstone facies (MF), overlying the LM and capped by the fine-grained laminated stromatolite facies (FLS). Note the coarser rudstone horizon, containing DR nodules, cutting across the MF approximately halfway through its thickness (white dotted lines). B) Thin section of the bioclastic packstone composing the MF, showing gastropod remains (yellow arrow) and pectinid fragments (green arrows). C) Outcrop view of the FLS facies resting on the DR and overlain by the Leuca Breccia deposits. D) Thin section of the FLS showing a mudstone texture with aligned fenestrae. E) Thin section of the FLS showing a packstone/wackestone rich in gastropod molds (blue arrows). F) Thin section of the FLS displaying a micro-laminated mudstone. (For interpretation of the references to colour in this figure legend, the reader is referred to the web version of this article.)

fluorescence, typically weak and diffuse, became noticeable under UV excitation at higher magnifications (≥200×), particularly in zones where the micrite exhibited a denser or more compact texture (Fig. 8F, G). The signal was markedly less intense than that observed in filaments and micrite clots within the ECF, but its presence was consistently observed across multiple thin sections.

In contrast, the recrystallized micrite of the type 2 packstone/grainstone does not exhibit fluorescence under UV-excitation. This non-fluorescent micrite appears more homogeneous in comparison to the fluorescent one and contains dispersed bio- and detrital clasts ranging from 50 μm to 2 mm in size. These components show no or only a weak luminescent response under UV-excitation.

5.4. SEM-EDS microfabric and chemical composition

Electron microscopy at high magnification allowed for detailed morphological characterization, showing distinct crystal habits of carbonate phases associated with the ECF filaments and surrounding

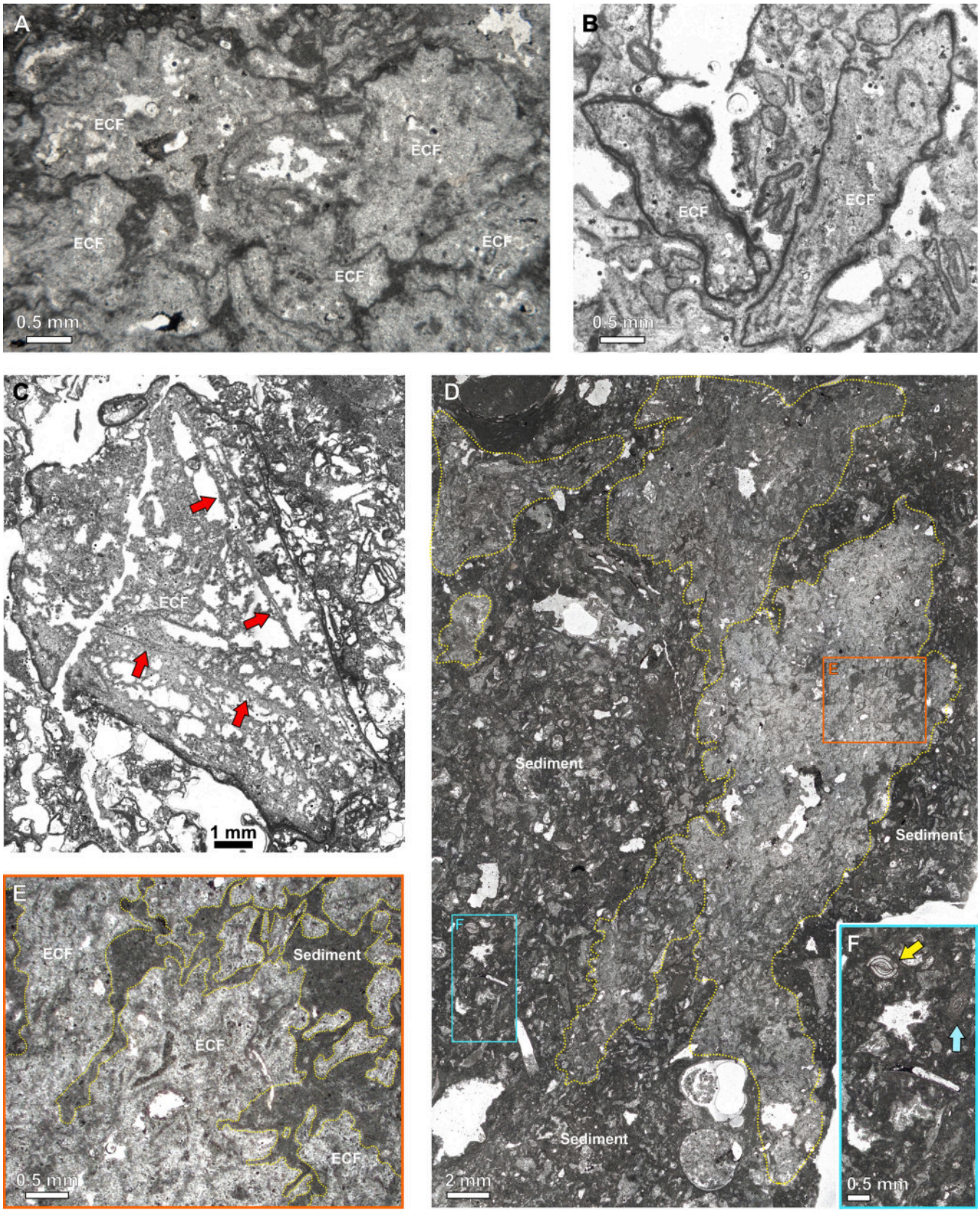

Fig. 6. A–C) ECF retaining most (A) or part (B, C) of their original shape; red arrows in C indicate the presence of filaments within their microstructure. D) ECF aggregates (outlined by yellow dotted lines) embedded in type 1 packstone. E) Close-up of D showing the arrangement of the ECF (outlined by yellow dotted lines) within the aggregate. F) Close-up of D highlighting the type 1 micrite with miliolids (yellow arrow) and echinoderm fragments (blue arrow). (For interpretation of the references to colour in this figure legend, the reader is referred to the web version of this article.)

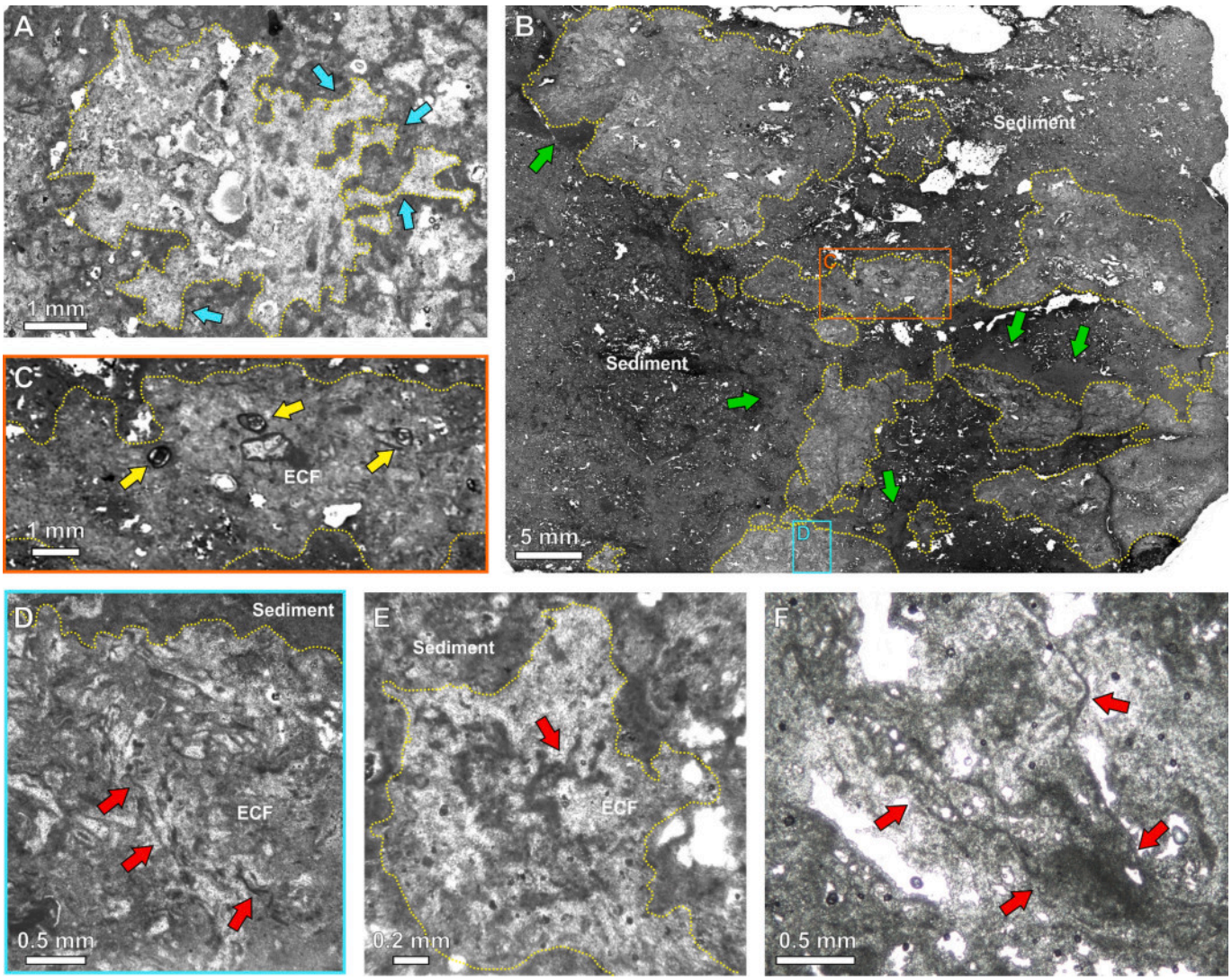

Fig. 7. A) Section of an ECF aggregate (outlined by yellow dotted lines) cut perpendicular to the main axis; note the irregular ramifications (blue arrows) radiating outward from a more compact central area. B) Large ECF aggregate (outlined by yellow dotted lines) with a widening-upward shape, embedded in type 1 packstone; green arrows indicate particularly dense, dark micritic crusts. C) Close-up of B showing an ECF (outlined by yellow dotted lines) incorporating small miliolids (yellow arrows) into its microstructure. D) Close-up of B showing an ECF (outlined by yellow dotted lines) containing dark filaments (red arrows) within the microstructure. E) ECF (outlined by yellow dotted lines) with evidence of dark, branching filaments (red arrow) within the microstructure. F) Detail of an ECF microstructure with filaments forming a branched tangle (red arrows). (For interpretation of the references to colour in this figure legend, the reader is referred to the web version of this article.)

micrite (Fig. 10), as well as those within the dark, peloidal micrite of the type 1 packstone and the recrystallized micrite of the type 2 packstone/grainstone.

SEM observations reveals that peloidal and aphanitic micrite within the ECF are characterized by a dense aggregate of fine-grained crystal fabric (Fig. 10A-C). This micrite engulf filamentous structures, while microcavities are partially filled by sparry and microsparitic cement with euhedral to subhedral crystal forms (Fig. 10A, B).

Filaments show diameters ranging from 20 to 30 μm, consistent with dimensions obtained through optical microscopy, and were identified within ECF structures by the distinct crystal characteristics of the filament walls, their internal fillings and the surrounding micrite (Fig. 10D-F). The nanocrystalline carbonate forming both the internal infillings of the filaments and their walls consists of poorly defined rhombohedral crystals ranging in size from 200 to 500 nm (Fig. 10E, F). Notably, wall crystals appear to exhibit a tangential alignment (Fig. 10F), whereas infilling crystals appear randomly oriented (Fig. 10E). The micrite surrounding the filaments (Fig. 11A) comprises larger anhedral to subeuhedral crystals (1–4 μm), organized in clots showing the same size and texture of the aphanitic to peloidal micrite observed in thin section. This micrite contains amorphous carbon-rich material (Fig. 11B), and very fine coccoid to bacilli-like corpuscles, measuring 50–100 nm in diameter and 100–500 nm in length (Fig. 11C). Minor tabular crystals are also scattered among rhombohedral calcite grains (Fig. 11C). Elongated, prismatic crystals, occasionally exhibiting pyramidal terminations, are observed within microcavities inside the micrite component of the ECF structures (Fig. 11D). These crystals display well-developed faces and range from isolated individuals to small aggregates. Their size varies from a few micrometers up to several tens of micrometers, and they are commonly oriented randomly within the host micrite.

In contrast, micrite and microsparite constituting the type 1 and type 2 packstone engulfing the ECF, show well-developed euhedral crystals significantly larger than those forming the filaments and associated micrite.

Elemental analysis shows that the microcrystals forming the walls of the filaments and those of the type 1 dark, peloidal micrite, have a low-

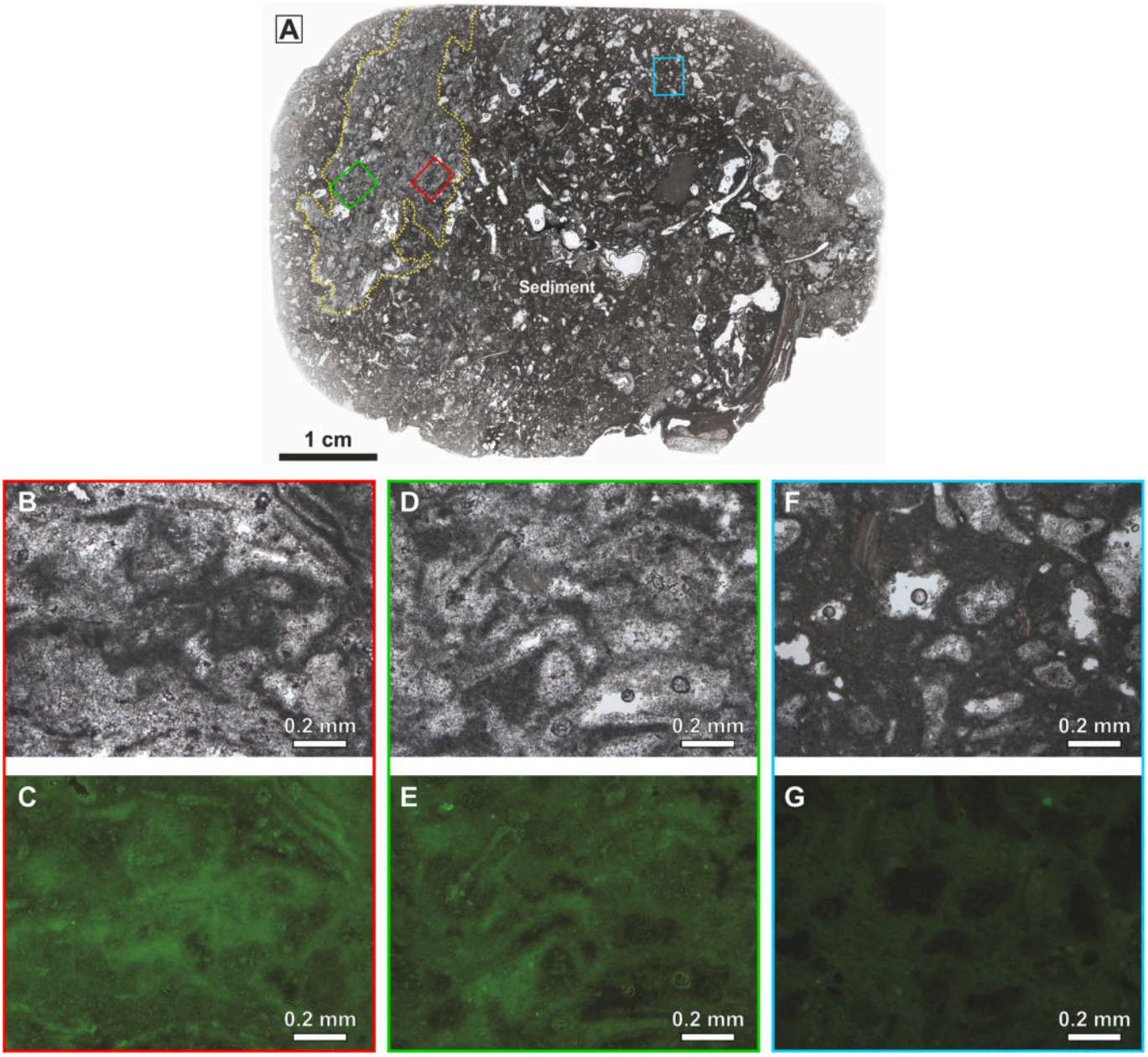

Fig. 8. A) Thin section showing an ECF aggregate (yellow dotted line) embedded in type 1 packstone matrix. B-E) Details of A with ECF filaments associated to micrite, note the high epifluorescence (C, E) of filaments and micrite. F-G) Details of A with type 1 packstone associated to the ECF aggregate in which micrite exhibits a weak epifluorescence. (For interpretation of the references to colour in this figure legend, the reader is referred to the web version of this article.)

magnesium calcium carbonate composition with subordinate silica content, as indicated by weak Si signals in the spectra. Additionally, the elongated, white prismatic crystals with pyramidal terminations contain S, Sr, and Ba, consistent with a mixed chemical composition of barite and celestine. The type 2 micrite also exhibits a low-magnesium calcium carbonate composition but presents higher concentrations of siliciclastic elements, evidenced by prominent Si and Al peaks.

6. Discussion

6.1. Origin and diagenesis of ECF and associated sediments

The mesoscale morphological features of the ECF suggest a potential biogenic origin. Their fan-shaped, lobed form indicates a possible link to biotic activity, an impression further supported by the morphology of the more complex structures described above. The vertically elongated aggregates, composed of interconnected individual ECF that resemble small upward- or laterally-oriented branches (Fig. 6D), closely match previously described examples of similar centimeter-scale, branched dendrolite fabrics (Riding, 1988, 1991, 2000). However, it is the occurrence of filaments within the ECF microstructure that allows a firmer recognition of their microbial origin. The diameter of the filaments (10–20 μm) and their length over several hundred micrometers are compatible with microbial structures, such as filamentous cyanobacteria or sulfur-oxidizing bacteria, which are commonly involved in microbially induced sedimentary structures (Riding, 2000; Noffke, 2010). These filaments are observable under transmitted light (Figs. 6C, 7D-F), but the combined use of this technique with UV-excitation (Fig. 9A, C, E) enhances their epifluorescence signal, revealing the details of the filament walls as well as submicron structures (<1 μm) that may correspond to preserved sheaths or mineralized exopolymeric substances (EPS) (Görgen et al., 2021). These fine-scale epifluorescent

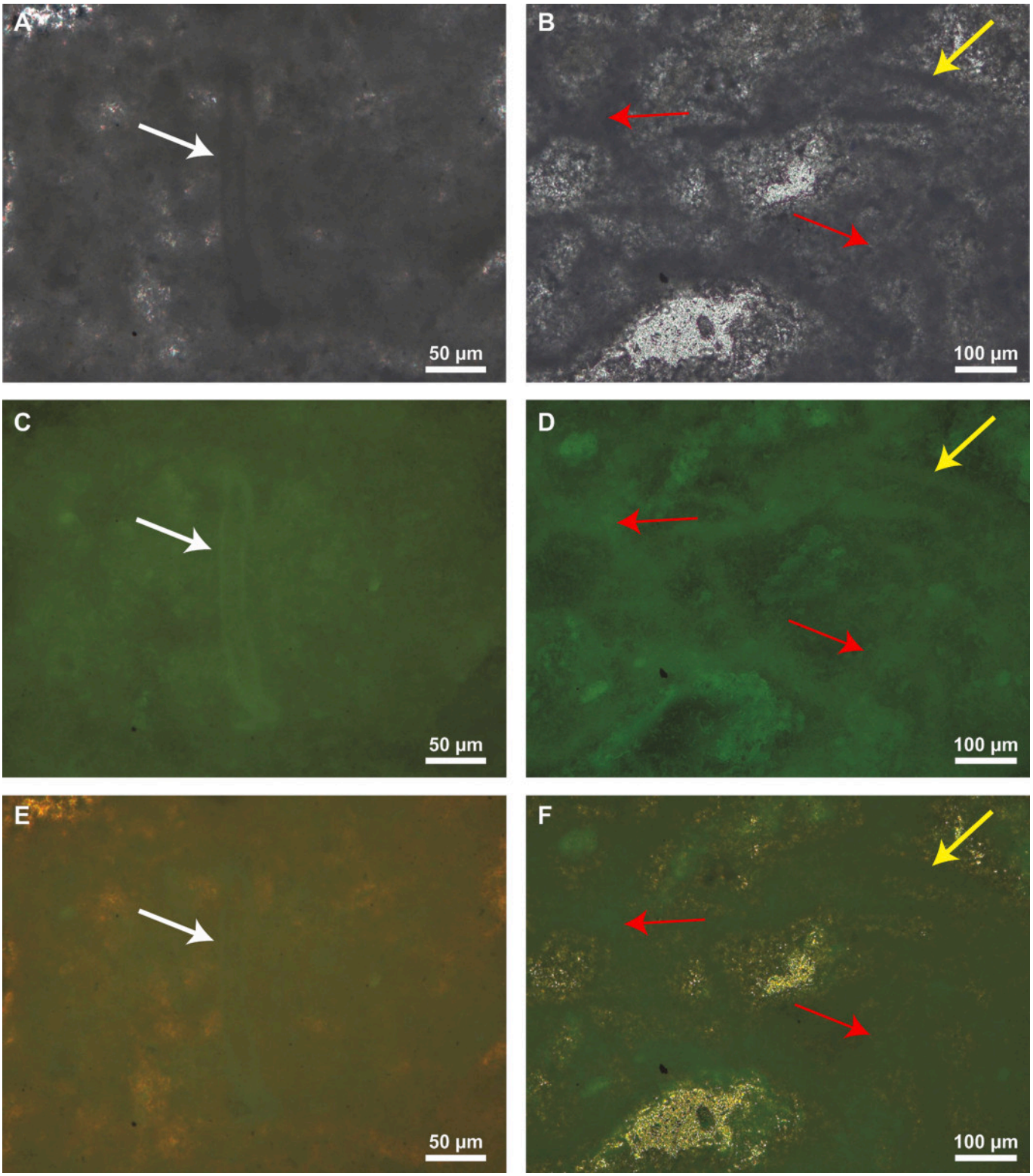

Fig. 9. Filaments (white arrows), filament walls (yellow arrows) and peloidal clots (red arrows) within ECF observed in: A, B) transmitted light; C, D) UV-Epifluorescence; and E, F) overlapping transmitted light and UV-Epifluorescence. The integration of visible light and UV-signal enhances the discrimination of the organic structures, allowing a pseudo-3D microscale visualization. (For interpretation of the references to colour in this figure legend, the reader is referred to the web version of this article.)

structures are indicative of the presence of organic material, potentially derived from microbial metabolism or cellular remnants (Neuweiler et al., 2000, 2003, 2023; Guido et al., 2022a, 2024; Cipriani et al., 2024). Moreover, the concentration of organic compounds within the core of peloids forming micritic clots within the ECF supports a model in which microbial activity played a role in the nucleation and early diagenesis of these carbonate particles. The irregular shape and size range (20–100 µm) of these clots are consistent with biomineralization processes

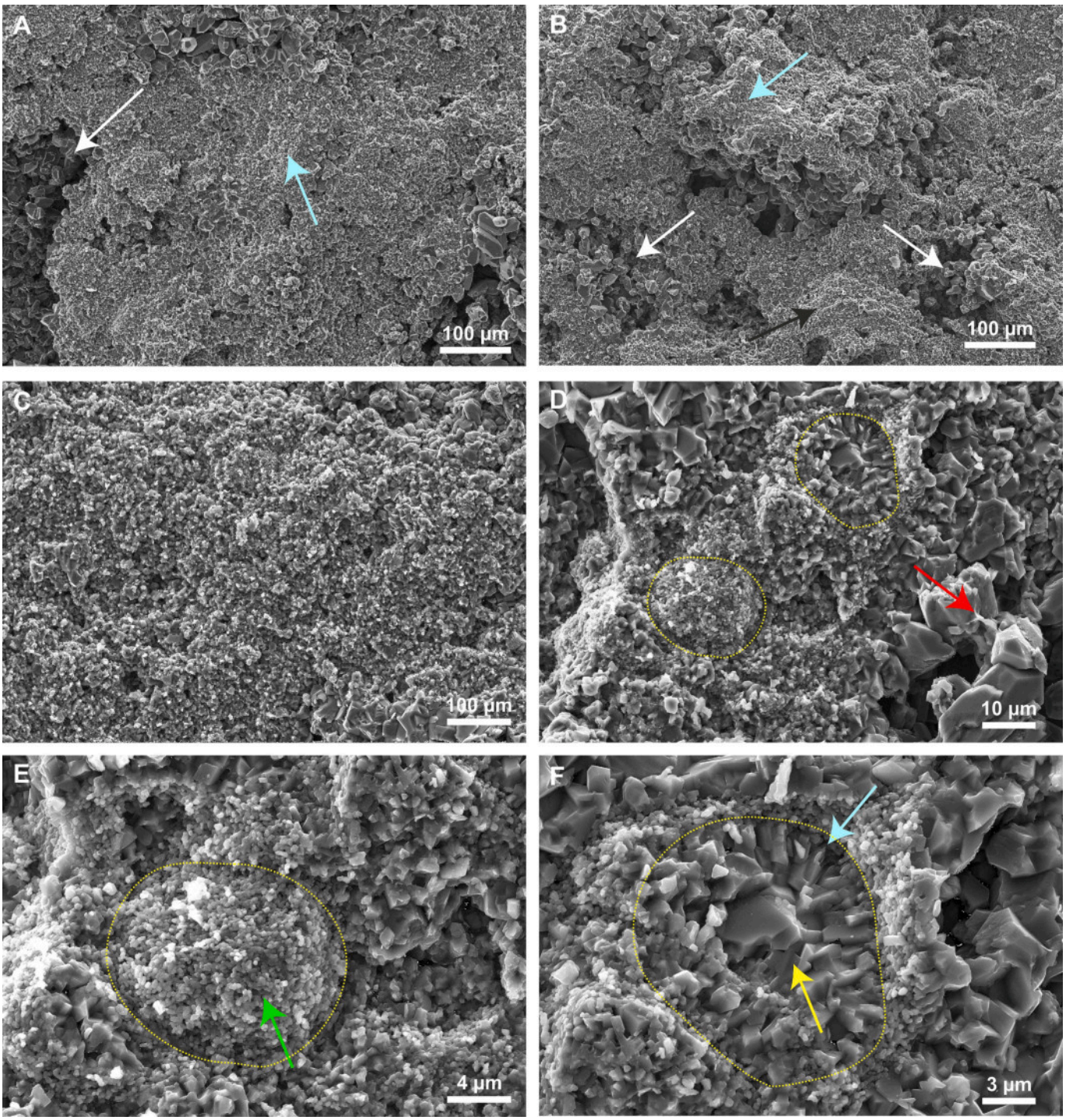

Fig. 10. SEM photomicrographs acquired on unpolished fragments of ECF. A, B) Very fine crystals of the peloidal and aphanitic micrite (blue arrows) engulfing filaments; larger crystals (white arrows) show microsparite and sparite cements filling microcavities. C) Detail of the autochthonous micrite crystals. D) Transversal section of filament remains (yellow dotted lines) engulfed in microsparite (red arrow). E, F) Details of the filaments (yellow dotted lines) showing the very fine texture of the walls composed of nanocrystals with a tangential arrangement (blue arrow in F); the filaments are filled of fine micrite (green arrow in E) or sparite crystals (yellow arrow in F). (For interpretation of the references to colour in this figure legend, the reader is referred to the web version of this article.)

associated with microbial mediation related to autotrophic and/or heterotrophic activities leading to *in situ* carbonate precipitation (Monty, 1976; Chafetz, 1986; Buczynski and Chafetz, 1991; Reitner, 1993; Pratt, 1995; Reitner and Neuweiler, 1995; Kazmierczak et al., 1996; Folk and Chafetz, 2000; Riding, 2000; Riding and Tomás, 2006; Guido et al., 2012, 2019, 2022b; Vescogni et al., 2008b, 2011). This spatial correlation between organic matter and micritic texture further reinforces the hypothesis of microbial mediation in the formation of the ECF structures.

The distinct difference in fluorescence response between filaments and micrite clots, and bioclastic-rich micrite forming the type 1 packstone, allows for a clear distinction between autochthonous components, resulting from *in situ* microbial activity, and allochthonous micritic particles of detrital origin (Cipriani et al., 2023, 2024). However, the weak fluorescence observed in the type 1, darkest portions of the micrite engulfing ECF may reflect the presence of a dispersed organic

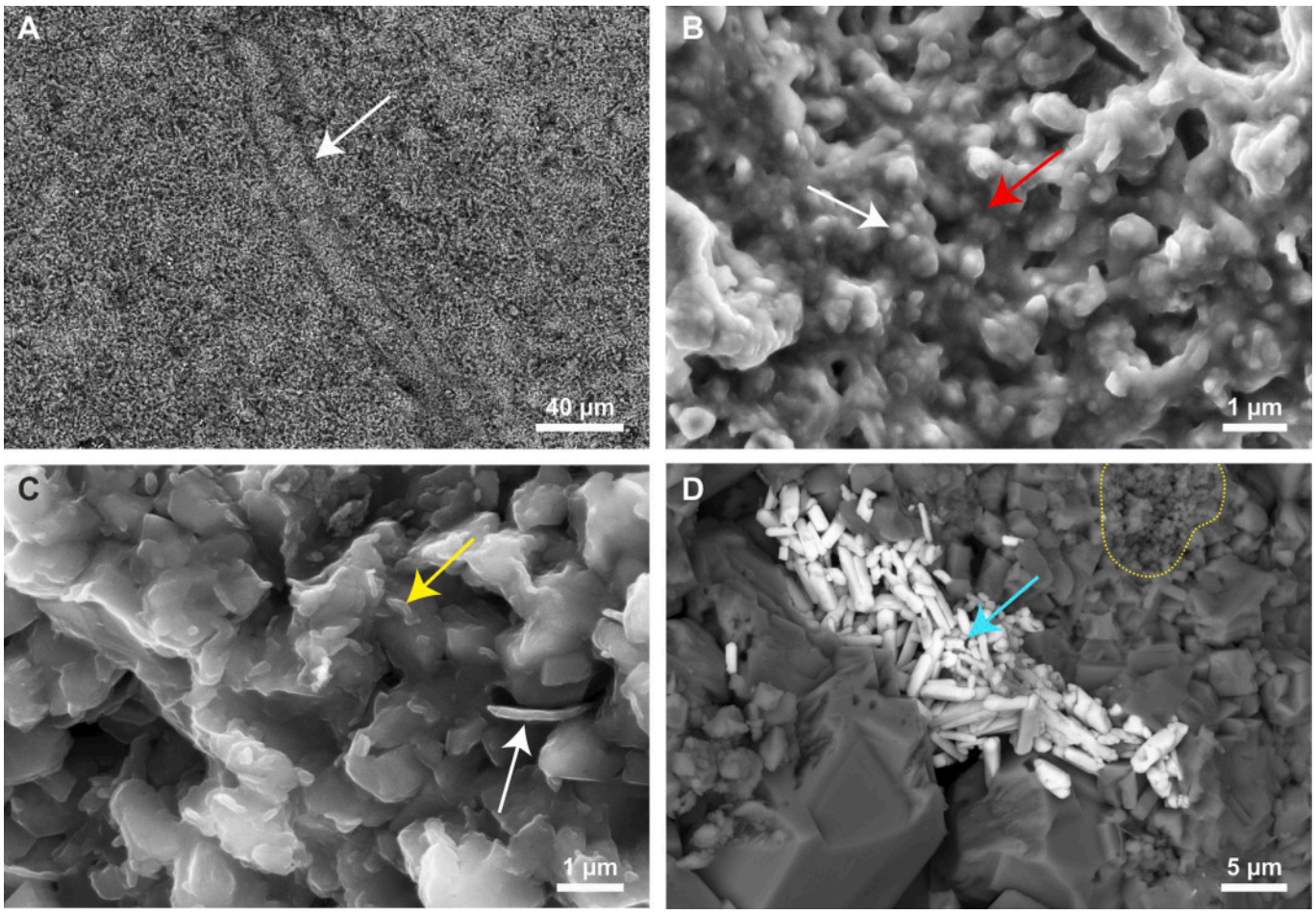

Fig. 11. SEM photomicrographs of an ECF acquired on thin section (A, B) and unpolished fragments (C, D). A) Same filaments (white arrow) showed in Figs. 9A, C and E; note the very fine crystals of the walls and engulfing peloidal micrite. B) Detail of the fine crystals of the filament walls; note the organic amorphous material (red arrow) which engulf the nanocrystals (white arrow). C) Detail showing clay minerals (white arrow) and very fine coccoid- to bacilli-like corpuscles (yellow arrow) strictly associated to autochthonous micrite components. D) Elongated, prismatic crystals (blue arrow), exhibiting pyramidal terminations, within microcavities inside the micrite component of the ECF structures; note the remains of putative filaments (yellow dotted line). (For interpretation of the references to colour in this figure legend, the reader is referred to the web version of this article.)

fraction trapped within the detrital micritic matrix (Guido et al., 2022b; Cipriani et al., 2024). This behavior indicates that, despite its allochthonous nature, the engulfing micrite preserve minor amounts of organic material, possibly derived from decayed microbial matter or incorporated during sedimentation. Such organic remnants may have acted as localized nucleation points, partially promoting microscale biomineralization processes even within the detrital fraction (Vescogni et al., 2022). While the extent of this contribution appears limited compared to the biogenic components of the ECF, the fluorescence signal supports the idea of a continuum between purely mechanical sedimentary inputs and organo-mineral interactions in the surrounding type 1 micritic matrix. Finally, the radically different behavior of type 2 micrite, with no traces of epifluorescence, testifies with its completely detrital origin, with no involvement of biomineralization processes.

The morphological and crystallographic features observed in electron microscopy suggest the occurrence of distinct processes also in the formation of the filamentous structures and the nearby micritic components within the ECF. The presence of nanometric rhombohedral crystals within the filament walls and fillings, coupled with their tangential and random orientations respectively, points to biologically mediated processes that facilitated carbonate precipitation under varying degrees of organic mediation (Reitner, 1993; Trichet and Défarge, 1995; Reid et al., 2000, 2003; Reitner et al., 2000; Dupraz et al., 2004, 2009; Decho et al., 2005; Dupraz and Visscher, 2005; Hendry et al., 2006; Braissant et al., 2007, 2009; Heindel et al., 2010). In particular, the tangential orientation of crystals composing the walls may reflect a templating effect exerted by microbial sheaths or by the extracellular polymeric substances (EPS), both commonly implicated in biomineralization processes (Görgen et al., 2021). Moreover, the close spatial association between amorphous carbon-rich material and the crystals of the peloidal micrite further supports a model of biomineralization (Benzerara et al., 2006, 2011; Dupraz et al., 2009). The fine corpuscular inclusions within the micrite (Fig. 11C) may represent degraded organic particles or microbial nanostructures, further reinforcing this interpretation (Benzerara et al., 2006; Usui et al., 2020; Guido et al., 2024). In addition, the heterogeneity of the type 1 packstone surrounding the dendroid structures, including skeletal and detrital grains larger than 10 µm, is consistent with episodic input of allochthonous material into the depositional environment. This may have influenced the local geochemistry, providing varying degrees of supersaturation and affecting microbial activity and carbonate precipitation dynamics (Vescogni et al., 2025). In contrast, the type 2 micrite and microsparite that have undergone recrystallization display more euhedral and significantly larger crystals, indicative of post-depositional diagenetic overprinting.

Concerning the EDS elemental analyses, the walls of the filament and the peloidal micrite intimately associated within the ECF structures display a low-magnesium calcium carbonate composition with minor

silica content, different to the type 1 detrital micrite engulfing the them, which exhibits a similarly low-magnesium composition but is enriched in siliciclastic elements, as evidenced by elevated Si and Al signals. These differing compositions again suggest a different origin of the two components, with ECF most probably produced *in situ* through an organic origin, whereas detrital micrite was imported from an external source.

The elongated, prismatic crystals with pyramidal terminations, found within microcavities of ECF and associated peloidal micrite (Fig. 11D), especially in more recrystallized areas, represent a secondary mineral phase distinct from the primary carbonate framework. The morphology, distribution and random orientation of these crystals suggest formation under diagenetic conditions within localized pore spaces. The presence of S, Sr, and Ba, suggests a mineralogy consistent with barite ($BaSO_4$) and celestine ($SrSO_4$). The localization of these sulfate minerals within ECF microcavities support their diagenetic origin (Guido et al., 2007; Sanz-Montero et al., 2009; Caruso et al., 2015). The occurrence of celestine may reflect processes of calcitization of an originally aragonitic composition of the ECF. Aragonite, being metastable under burial conditions, is commonly replaced by calcite during diagenesis, and sulfate minerals such as celestine can precipitate due to the release of strontium within pore spaces during replacement of aragonite.

The data presented thus far lead us to interpret the ECF as biotic structures, originally aragonitic, and likely associated with biomineralization processes mediated by putative filamentous cyanobacterial communities. In particular, the morphology and size of the related aggregates closely resemble those of dendrolites, with the ECF representing remnants of branches forming elliptical, vertically elongated dendroids (*sensu* Shapiro and Wilmeth, 2020) (Fig. 12A).

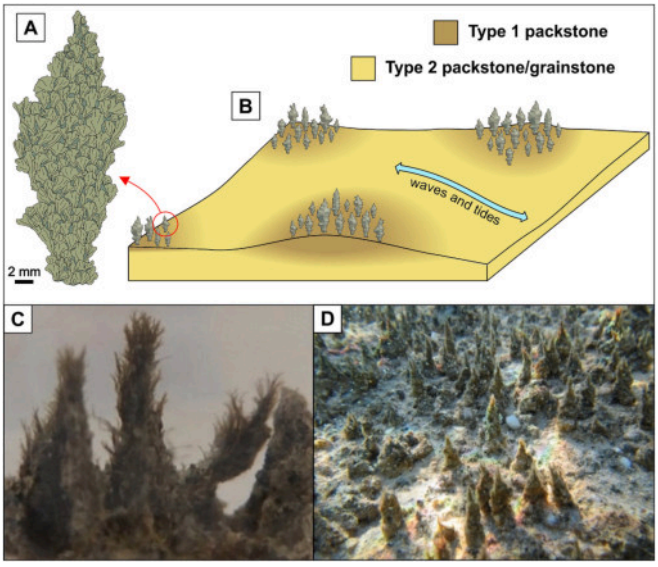

Fig. 12. A) Reconstruction of a Messinian dendroid formed by the interconnection of numerous small branches (ECF). B) Tentative reconstruction of the Messinian dendrolite depositional system. The dendroids were possibly arranged in small clusters, promoting the deposition of type 1 packstone through trapping and binding, whereas the intervening areas were filled with loose sediment kept in motion by waves and tides, leading to the formation of type 2 packstone/grainstone. C) Detail of a present-day Hamelin Pool dendroid cluster, showing their vertically elongated shape and filamentous arrangement; maximum dendroid height is 3 cm. D) Overview of a Hamelin Pool dendroid colonization, with dendroids occurring either individually or in small clusters surrounded by patches of loose sediment; maximum dendroid height is 3 cm. C and D modified from Suosaari et al. (2018).

6.2. *Comparisons with fossil and present-day dendrolites*

6.2.1. *Dendrolite types and main features*

As already stated, following the original definition of Riding (1988, 1991, 2000), dendrolites are macroscopically non-laminated deposits, related to microbial induced calcification and with a prevalent centimetric, dendritic fabric. At the microfabric scale, dendrolites exhibit highly variable assemblages, often lacking well-defined boundaries. In general terms, based on their microfabric, four distinct dendrolite types can be distinguished:

a) Sparry dendrolites, also known as dendrites, consist of some cm tall, branched growth-forms with a micritic core surrounded by fibrous/sparry calcite (Fig. 2 in Frasier and Corsetti, 2003). They are relatively rare in Proterozoic shallow-water marine platforms (Sami and James, 1996; Pope and Grotzinger, 2000; Frasier and Corsetti, 2003; Riding, 2008). They have been considered as products of abiotic precipitation (Sami and James, 1996; Pope and Grotzinger, 2000) as well as biogenic structures related to the presence of microbial communities (Frasier and Corsetti, 2003).

b) Clotted dendrolites are characterized by a microfabric made by the interconnection of small micritic clots, with spherical, elongated or more irregular shapes (Fig. 2 in Lee et al., 2015). They are widespread mainly from the Cambrian to the Early Ordovician, with phases of resurgence during the Late Devonian and at the Permian–Triassic boundary. In some cases, they were principally produced by calcimicrobes, primarily *Epiphyton*, *Renalcis*, *Angusticellularia* and other subordinate taxa. Most clotted dendrolites seem to occur in shallow-water marine environments, where they acted as important components of reef structures, alone or in association with metazoans (Riding, 1991, 2000; Rowland and Shapiro, 2002; Shapiro and Rigby, 2004; Kershaw et al., 2007, 2012; Woo et al., 2008: Howell et al., 2011; Lee et al., 2015; Wu et al., 2017).

c) Microlaminated dendrolites, as their name suggests, exhibit a finely laminated microfabric, typically characterized by the alternation of dark and light laminae (Fig. 9C in Ibarra et al., 2014). They have been considered as the products of biomineralization mediated by microbial communities and appear to be less common in the fossil record compared to the clotted type. Notable examples have been reported from the late Cambrian to Early Ordovician of Texas, where they occur as short, thick-branched growth forms that developed in shallow-water, high-energy, normal marine environments (Lee and Riding, 2023). Upper Triassic microlaminated dendrolites from south-west Britain are small, finely digitate structures alternate with stromatolitic layers and are thought to have formed in shallow water under high pCO_2 and warm conditions (Ibarra et al., 2014). A more recent example is represented by microlaminated dendrolites from the same Salento, upper Messinian outcrop considered in the present study. These are centimetric dendritic growth forms, that formed a large, meter-scale buildup in a shallow-water lagoon, under moderate to high energy, variable salinity, and a high sedimentation rate (Vescogni et al., 2025).

d) Filamentous dendrolites, commonly shrub-like or tufted, are arborescent, elongate structures, a few centimeters in maximum height, with a microfabric mainly made by upward-oriented tangles of cyanobacteria filaments (Fig. 12C). They may display a variety of arrangements, with varied degrees of ramifications and with branches that may radiate from a single point or split from a common stem (Claes et al., 2017). These dendrolites usually have a low degree of calcification and thus a very limited preservation potential, so only present-day examples are known. Examples have been mainly described from hydrothermal, hypersaline or in any case super-saturated environments, *e.g.*, in coastal, shallow-water hypersaline lagoons in Laguna Mormona (Horodyski et al., 1977) and Laguna Guerrero Negro (Javor and Castenholz, 1981) in Mexico. They are also known from a salina in Hainan Island, China (Zhang and Hoffmann, 1992), and from Hamelin Pool, Western Australia, where they form ephemeral growth-forms within the mid to lower intertidal zone (Suosaari et al., 2018). Filamentous dendrolites

have also been recorded in other continental settings, such as a high-altitude hypersaline lake in the Catamarca region, north-west Argentina (Lencina et al., 2021), a shallow geothermal pool at Little Hot Creek, California (Bradley et al., 2017) and a hypersaline lake in Andros Island, Bahamas (Monty, 1972).

6.2.2. Comparison between Hamelin Pool and Salento Messinian dendrolites

From a microfabric point of view, the upper Messinian dendrolites described here fall within the filamentous dendrolite type and, in particular, show strong similarities to the present-day examples described from Hamelin Pool (Suosaari et al., 2018). The following summary is taken from Suosaari et al. (2018), to which the reader is referred for a more detailed account.

Hamelin Pool is a shallow-water embayment with limited water circulation, hypersaline conditions, and considerable annual variations in temperature and water level. These fluctuating conditions result in a reduced number of grazers, allowing microbial communities to thrive. In Hamelin Pool, dendrolites are ephemeral and occur only during the warmer summer months, when they colonize the mid- to lower intertidal zone, forming meter-scale patches characterized by small concentrations alternating with areas covered by sediment (Fig. 12D).

The Hamelin Pool dendrolites exhibit a non-laminated, branching growth-form composed of clumps of cyanobacteria. They lack a distinct axial zone and display a vertically elongated, bushy morphology, reaching a maximum height of 3 cm (Fig. 12C). They are primarily composed of *Lyngbya aestuarii* and *Lyngbya fragilis*, with maximum sheath thicknesses of 40 μm and 30 μm, respectively, and are seasonally associated with smaller amounts of diatoms as well as other filamentous and coccoid cyanobacteria. In particular, *L. aestuarii* forms the main vertical trunk, while *L. fragilis* and the other cyanobacterial taxa produce secondary branches that radiate outward. The entire structure is surrounded by EPS and trapped sediment grains. Hamelin Pool dendrolites appear to lack carbonate precipitation and therefore have no preservation potential.

A precise comparison between the upper Messinian dendrolites and those of Hamelin Pool is clearly hindered by the absence, in the former case, of well-preserved structures at the outcrop scale. However, many of the key distinguishing features of these two examples are remarkably similar. At the mesofabric level, their overall morphology, size, and subdivision into a more compact central core surrounded by outward-extending branches show strong convergence. The same applies to the dimensions: the filaments are comparable in size, measuring 20–30 μm in the Messinian dendrolites and up to 30–40 μm in the Hamelin Pool examples. In both cases, filaments appear as individual strands, either straight or variably oriented, or arranged in irregularly coiled clusters. The taxonomic attribution of the Messinian filaments cannot be established based solely on morphological features. However, their similar size with the Hamelin Pool analogues permits the hypothesis that *Lyngbya*-like microbial communities may have been involved in the formation of the Messinian ECF fabric. Furthermore, the presence of highly fluorescent micrite associated with the fossil dendroids could be related to decay of organic matter nested among their filaments. These organic compounds are likely comparable to the EPS observed surrounding the filaments in the modern examples.

A further similarity between the two dendrolite examples comes from the analysis of type 1 packstone associated with the Messinian dendroids. This sediment is rich in bioclasts and contains dense, dark micrite exhibiting a weak epifluorescence, suggesting a link to the presence of organic matter. Analogously, the EPS coating the filaments of the Hamelin Pool dendroids contributes to the trapping of sedimentary grains and, possibly, of external organic matter associated with the detrital material. This organic matrix could play a role in microscale biomineralization processes, also contributing to the binding of the sedimentary particles.

A notable difference, however, is the lack of mineralization in the Hamelin Pool dendrolites, in contrast to the originally aragonitic, lobate branches that characterize the Messinian analogues.

The degree of dendrolite mineralization, and, more broadly, that of microbialites in general, depends on multiple factors, generally related to the type of microbial association and to physicochemical conditions operating at both macro- and micro-scale (Riding and Virgone, 2020). It is therefore not simple to identify a precise factor responsible for Messinian dendrolite mineralization, since it could be a combination of a wide variety of differing parameters, including palaeoenvironmental factors (*e.g.* temperature, pCO_2, hydrodynamic conditions), alkalinity, availability of free calcium, and the precise type of microbial community involved in the biomineralization process, as well as their metabolism.

Finally, it is not possible to compare the macroscopic features of these two examples, since the shape, size, and lateral extent of the Messinian colonizations have not been preserved. We interpret the massive, nodular appearance of the DR facies, containing nearly all of the dendrolites described here, as the result of intense reworking. The type 1 packstone and type 2 packstone/grainstone in the DR facies (Fig. 4G, H) differ in their type of micrite, textures and bioclastic assemblages, suggesting distinct depositional processes. However, they occur closely intermixed without any spatial pattern. This random distribution supports the interpretation that originally adjacent heteropic sedimentary deposits were mixed prior to diagenesis. The extremely chaotic appearance of the DR facies hinders the identification of the specific processes responsible for its arrangement, making any interpretation quite speculative. One possible explanation involves storm or flood events occurring within a confined, protected environment. Such events may have promoted repeated winnowing, short-distance transport, and local redeposition of sediments. In this scenario, the disruption of carbonate bodies with varying degrees of early lithification could have resulted in the formation of nodules dispersed within a more compact matrix. However, another plausible explanation may be related to bioturbation. Despite the absence of evident trace fossils, the nodular appearance of the DR facies could result from particularly intense burrowing activity by infaunal organisms. In this process, burrows would become intertwined and mixed, creating a complex sedimentary arrangement with heterogenous porosity, ultimately leading to the formation of more porous nodules associated to denser matrix.

6.3. Depositional model

Based on the depositional geometries and the carbonate grain association, including miliolids, dasycladacean and coralline red algae, *Porites* corals and ooids, Vescogni et al. (2022) interpreted the SP-TCC depositional system as a proximal, shallow-water environment under tropical/sub-tropical climate conditions. In particular, the stratigraphic interval investigated in the present study has been interpreted as a small lagoon, possibly protected from the open sea by the presence of oolite grainstone shoals and/or small *Porites* bioconstructions.

Based on the data here presented, the basal LM facies can be linked to very low hydrodynamic conditions, as indicated by the prevalent microlaminated mudstone. Furthermore, the nearly complete absence of bioclasts and bioturbation, as well as the likely presence of organic matter concentrations, suggest a highly stressed environment, possibly resulting from very limited connections with the open sea, which may have led to salinity and/or oxygen imbalances.

The nature of the irregular erosional surface separating the LM facies from the overlying SML (Fig. 3) is not entirely clear: it could be related to high-frequency oscillation of relative sea-level, to changes in the connections with the open sea, or to a storm event. In any case, the SML palaeoenvironment seems broadly similar to that of the LM. Both facies are characterized by fine-laminated mudstones. However, in the SML the occurrence of pellets, gastropods, small benthic foraminifera, as well as traces of bioturbation, suggests a less stressed environment. These conditions also allowed for colonization by microbial communities. The presence of micritic laminae with aligned fenestrae (Fig. 4D) can be

possibly interpreted as the result of microbially induced calcification, and the first occurrence of few, scattered dendroids suggests at least the presence of suitable oxygen levels.

The origin of the abrupt erosional surface connecting SML to DR facies is not easy to reconstruct, and the same explanations proposed for the underlying boundary can also be invoked in this case. The reconstruction of the DR facies palaeoenvironment, which represents the principal depositional setting of the Messinian dendrolites, is likewise not straightforward, mainly because, as previously mentioned, the original sedimentary features appear to have been heavily disrupted. Nevertheless, some information can be derived from the bioclastic fraction of the type 1 packstone engulfing the dendrolites. The occurrence of a diversified biotic assemblage, containing gastropods, oysters, ostracods, and small benthic foraminifera such as miliolids, some species of *Elphidium* and *Ammonia*, and especially echinoids suggests a palaeoenvironment that, compared with the previous facies, begins to approximate normal marine conditions, in particular with respect to salinity. Further insight into DR depositional dynamics, particularly regarding the different origins of the type 1 packstone and type 2 packstone/grainstone, may be gained through comparison with the depositional setting of Hamelin Pool dendrolites. Hamelin Pool colonizations clearly reveal the presence of two distinct areas arranged into irregular patches: a) those occupied by dendroids, either isolated or clustered, and b) those filled by loose sediment (Fig. 12D). These two areas can be regarded as distinct sub-settings of the depositional environment. In the first case the filaments of the Hamelin Pool dendroids, which are often coated by EPS, contribute to the trapping of fine-grained sedimentary particles (Suosaari et al., 2018) and, possibly, of external organic matter associated with bioclastic grains. A similar dynamic, as already mentioned, can be tentatively proposed for the Messinian examples, facilitating the formation of the type 1 packstone (Fig. 12B). Moreover, as in the Hamelin Pool depositional setting, the possible presence of areas occupied by loose sediment among the Messinian dendroids could explain the formation of the type 2 packstone/grainstone. The occurrence of patches and small channels devoid of dendroids, associated with the action of waves a tides, may have promoted the formation of grain-supported deposits (Fig. 12B) characterized by non-fluorescent micrite of detrital origin. In any case, the hydrodynamic conditions were likely not too strong, given the fragile structures of the nearby dendroids. The ooid-like crusts often coating the detrital grains (Fig. 4H, I) further support the presence of tropical climatic conditions, as previously suggested by Vescogni et al. (2022).

The onset of the MF facies terminated the colonization by dendroids. The depositional geometries of the MF facies (Fig. 3) suggest abrupt formation of a channel, incised into the DR and underlying facies, possibly related to a storm event. The occurrence of such an event is supported by vertical gradation of the sedimentary textures within the MF facies, which pass upward from a dominant packstone to mud-supported deposits, as well as by the presence of a distinct rudstone horizon cutting across the MF deposits and containing nodules (Fig. 5A) that are clearly derived from the erosion of the DR facies flank. The absence of dendroid colonization can thus be explained by the high-energy nature of the MF facies, possibly related to one or more erosive events, followed by infilling of the resulting channel by sediments of detrital origin.

The DR and MF deposits gradually pass into the FLS facies, the latter being characterized by superimposition of thin layers with different textures. These include: fine-grained stromatolitic horizons, with typical micritic layers rich in fenestrae and associated with calcite laminae; bioclastic packstone/wackestone containing gastropods, pellets, miliolids, rare echinoderms and serpulids; and nearly barren, microlaminated mudstone (Fig. 5C–F). On the whole, these sediments suggest a return to low-energy conditions, though possibly characterized by periodic oscillations in key paleoenvironmental factors such as salinity and oxygen (Vescogni et al., 2022). These fluctuations may have been linked to changes in connections with the open sea, and could have been responsible for the alternation among the types of textures described above: stromatolites and barren mudstone, associated with restricted conditions, and bioclastic packstone/wackestone, reflecting a palaeoenvironment closer to normal marine settings. Alternatively, the bioclastic packstone/wackestone could be interpreted as deposited within a restricted environment following high-energy events (storms).

7. Conclusions

Small carbonate aggregates in upper Messinian deposits in the Salento Peninsula, central Mediterranean, consist of vertically elongated growth-forms, a few centimeters tall, made up of interconnected small, fan-like, lobate structures. Within these structures, filamentous remains have been observed, comparable in size and shape to present-day cyanobacterial microstructures.

The size and shape of these aggregates, together with evidence of filaments and organic-derived micrite within their microfabrics, suggest a microbial, cyanobacterial, origin. In particular they closely resemble filamentous dendrolites, and are compared with present-day analogues in Hamelin Pool, western Australia.

The sediments containing the Messinian dendroids, and more generally the facies association forming the entire depositional system, indicate a palaeoenvironment represented by a small lagoon, characterized by conditions fluctuating over time from restricted to open-marine, possibly due to unstable connections with the open sea.

Detailed palaeoenvironmental reconstruction of the dendrolite facies is difficult because its original sedimentary organization has been largely obliterated. A tentative interpretation, has been based on the prevalent sedimentary textures and bioclastic assemblages, together with comparison with the Hamelin Pool depositional environment. On this basis, the Messinian dendroids are thought to have formed in a very shallow-water setting, under warm climatic conditions and moderate hydrodynamics, with water chemistry similar to normal marine values.

Salento filamentous dendrolites are the first finding of this microbialite type in the fossil record. This is most probably related to their higher degree of mineralization compared to present-day analogues, which led to the formation of an originally aragonitic microfabric.

Declaration of generative AI and AI-assisted technologies in the manuscript preparation process

During the preparation of this work the authors used ChatGPT in order to improve the English language. After using this tool/service, the authors reviewed and edited the content as needed and take full responsibility for the content of the published article.

CRediT authorship contribution statement

Alessandro Vescogni: Writing – original draft, Visualization, Methodology, Investigation, Funding acquisition, Formal analysis, Data curation, Conceptualization. **Adriano Guido:** Writing – original draft, Visualization, Methodology, Investigation, Formal analysis, Data curation, Conceptualization.

Declaration of competing interest

The authors declare no conflicts of interest.

Acknowledgments

We thank the Editor, Lucia Angiolini, and the Guest Editor, Juan Carlos Braga, for their helpful guidance and suggestions. We are also grateful to two anonymous reviewers for their constructive comments, which greatly improved the manuscript. We would like to thank Andrea Baucon for his valuable suggestions regarding the nature of the sedimentary structures in the dendrolite-bearing facies. Partial support was

provided to A. Vescogni through "FAR 2024"—Dipartimento di Scienze Chimiche e Geologiche, University of Modena and Reggio Emilia grants.

Data availability

All data are reported in the article.

References

André, J.P., Cornée, J.J., Saint Martin, J.P., Lapointe, P., 2002. Organisation séquentielle de la plate-forme carbonatée messinienne du seuil pélagien à Lampedusa (Méditerranée centrale). In: Néraudeau, D., Goubert, E. (Eds.), l'Événement messinien: approches paléobiologiques et paléoécologiques, 24(3). Geodiversitas, pp. 625–639.

Benzerara, K., Menguy, N., López-García, P., Yoon, T.H., Kazmierczak, J., Tyliszczak, T., Guyot, F., Brown, G.E., 2006. Nanoscale detection of organic signatures in carbonate microbialites. Proc. Natl. Acad. Sci. 103, 9440–9445.

Benzerara, K., Miot, J., Morin, G., Ona-Nguema, G., Skouri-Panet, F., Ferard, C., 2011. Significance, mechanisms and environmental implications of microbial biomineralization. Compt. Rendus Geosci. 343, 160–167.

Bosellini, F.R., 2006. Biotic changes and their control on Oligocene–Miocene reefs: a case study from the Apulia Platform margin (southern Italy). Palaeogeogr. Palaeoclimatol. Palaeoecol. 241, 393–409.

Bosellini, A., Bosellini, F.R., Colalongo, M.L., Parente, M., Russo, A., Vescogni, A., 1999. Stratigraphic architecture of the Salento coast from Capo d'Otranto to S. Maria di Leuca (Apulia, southern Italy). Riv. Ital. Paleont. Stratigr. 105, 397–416.

Bosellini, F.R., Russo, A., Vescogni, A., 2001. Messinian reef-building assemblages of the Salento Peninsula (southern Italy): palaeobathymetric and palaeoclimatic significance. Palaeogeogr. Palaeoclimatol. Palaeoecol. 175, 7–26.

Bosellini, F.R., Russo, A., Vescogni, A., 2002. The Messinian reef complex of the Salento Peninsula (Southern Italy): stratigraphy, facies and paleoenvironmental interpretation. Facies 47, 91–112.

Bosellini, F.R., Vescogni, A., Budd, A., Papazzoni, C.A., 2021. High coral diversity is coupled with reef-building capacity during the late Oligocene warming (Castro Limestone, Salento Peninsula, S Italy). Riv. Ital. Paleontol. Stratigr. 127 (3), 515–538.

Bossio, A., Mazzei, R., Monteforti, B., Salvatorini, G., 2002. Note illustrative alla carta geologica della zona di S. Maria di Leuca. Atti Soc. Toscana Sci. Nat. Mem. 107, 97–163.

Bourillot, R., Vennin, E., Dupraz, C., Pace, A., Foubert, A., Rouchy, J.M., Patrier, P., Blanc, P., Bernard, D., Lesseur, J., Visscher, P.T., 2020. The record of environmental and microbial signatures in ancient microbialites: the Terminal Carbonate Complex from the Neogene basins of southeastern Spain. Minerals 10, 276.

Brachert, T.C., Vescogni, A., Bosellini, F.R., Reuter, M., Mertz-Kraus, R., 2007. High salinity variability during the early Messinian revealed by stable isotope signatures from vermetid and *Halimeda* reefs of the Mediterranean region. Geol. Romana 40, 51–66.

Bradley, J.A., Daille, L.K., Trivedi, C.B., Bojanowski, C.L., Stamps, B.W., Stevenson, B.S., Nunn, H.S., Johnson, H.A., Loyd, S.J., Berelson, W.M., Corsetti, F.A., Spear, J.R., 2017. Carbonate-rich dendrolitic cones: insights into a modern analog for incipient microbialite formation, little Hot Creek, Long Valley caldera, California. NPJ Biofilms Microbiomes 3, 32.

Braga, J.C., Martin, J.M., Riding, R., 1995. Controls on microbial dome fabric along a carbonate-siliciclastic shelfbasin transect, Miocene, SE Spain. Palaios 10, 347–361.

Braga, J.C., Vescogni, A., Bosellini, F.R., Aguirre, J., 2009. Coralline algae (Corallinales, Rhodophyta) in western and Central Mediterranean Messinian reefs. Palaeogeogr. Palaeoclimatol. Palaeoecol. 275, 113–128.

Braissant, O., Decho, A.W., Dupraz, C., Glunk, C., Przekop, K.M., Visscher, P.T., 2007. Exopolymeric substances of sulfate-reducing bacteria: interactions with calcium at alkaline pH and implication for formation of carbonate minerals. Geobiology 5, 401–411.

Braissant, O., Decho, A.W., Przekop, K.M., Gallagher, K.L., Glunk, C., Dupraz, C., Visscher, P.T., 2009. Characteristics and turnover of exopolymeric substances in a hypersaline microbial mat. FEMS Microbiol. Ecol. 67, 293–307.

Buczynski, C., Chafetz, H.S., 1991. Habit of bacterially induced precipitates of calcium carbonate and the influence of medium viscosity on mineralogy. J. Sediment. Petrol. 61, 226–233.

Calvet, F., Zamarreno, I., Valles, D., 1996. Late Miocene reefs of the Alicante-Elche basin, southeast Spain. In: Franseen, E.K., Esteban, M., Ward, W.C., Rouchy, J.M. (Eds.), Models for Carbonate Stratigraphy from Miocene Reef Complexes of Mediterranean Region, vol. 5. SEPM Concept. Sedimentol. Paleontol, pp. 177–190.

Caruso, A., Pierre, C., Blanc-Valleron, M.M., Rouchy, J.M., 2015. Carbonate deposition and diagenesis in evaporitic environments: the evaporative and sulphur-bearing limestones during the settlement of the Messinian salinity crisis in Sicily and Calabria. Palaeogeogr. Palaeoclimatol. Palaeoecol. 429, 136–162.

Chafetz, H.S., 1986. Marine peloids: a product of bacterially induced precipitation of calcite. J. Sediment. Petrol. 56, 812–817.

Cipriani, M., Basso, D., Bazzicalupo, P., Bertolino, M., Bracchi, V.A., Bruno, F., Costa, G., Dominici, R., Gallo, A., Muzzupappa, M., Rosso, A., Perri, F., Sanfilippo, R., Sciuto, F., Guido, A., 2023. The role of non-skeletal carbonate component in Mediterranean Coralligenous: new insight from the CRESCIBLUREEF project. Rend. Online Soc. Geol. It. 59, 75–79.

Cipriani, M., Apollaro, C., Basso, D., Bazzicalupo, P., Bertolino, M., Bracchi, V.A., Bruno, F., Costa, G., Dominici, R., Gallo, A., Muzzupappa, M., Rosso, A., Sanfilippo, S., Sciuto, F., Vespasiano, G., Guido, A., 2024. Origin and role of non-skeletal carbonate in coralligenous build-ups: new geobiological perspectives in biomineralization processes. Biogeosciences 21, 49–72.

Claes, H., Marques-Erthal, M., Soete, J., Özkul, M., Swennen, R., 2017. Shrub and pore type classification: petrography of travertine shrubs from the Ballık-Belevi area (Denizli, SW Turkey). Quat. Int. 217, 147–163.

Cornée, J.J., Saint Martin, J.P., Conesa, G., Munch, P.H., André, J.P., Saint, Martin S., Roger, S., 2004. Correlations and sequence stratigraphic model for Messinian carbonate platforms of the western and central Mediterranean. Int. J. Earth Sci. 93, 621–633.

Dabrio, C.J., Polo, M.D., 1995. Oscilaciones eustaticas de alta frecuencia en el Neogeno superior de Sorbas (Sorbas, sureste de Espana). Geogaceta 18, 75–78.

Decho, A.W., Visscher, P.T., Reid, R.P., 2005. Production and cycling of natural microbial exopolymers (EPS) within a marine stromatolite. Palaeogeogr. Palaeoclimatol. Palaeoecol. 219, 71–86.

Dunham, R.J., 1962. Classification of carbonate rocks according to depositional texture. In: Hamm, W.E. (Ed.), Classification of Carbonate Rocks, A Symposium, vol. 1. AAPG Mem, pp. 108–121.

Dupraz, C., Visscher, P.T., 2005. Microbial lithification in marine stromatolites and hypersaline mats. Trends Microbiol. 13, 429–438.

Dupraz, C., Visscher, P.T., Baumgartner, L.K., Reid, R.P., 2004. Microbe mineral interactions: early carbonate precipitation in a hypersaline lake (Eleuthera Island, Bahamas). Sedimentology 51, 745–765.

Dupraz, C., Reid, R.P., Braissant, O., Decho, A.W., Norman, R.S., Visscher, P.T., 2009. Processes of carbonate precipitation in modern microbial mats. Earth Sci. Rev. 96, 141–162.

Embry, A.F., Klovan, J.E., 1971. A Late Devonian reef tract on Northeastern Banks Island, N.W.T. B. Can. Petrol. Geol. 19, 730–781.

Esteban, M., 1979. Significance of the upper miocene coral reefs of the western Mediterranean. Palaeogeogr. Palaeoclimatol. Palaeoecol. 29, 169–188.

Feldmann, M., McKenzie, J.A., 1997. Messinian stromatolite-thrombolite associations, Santa Pola, SE Spain: an analogue for the Palaeozoic? Sedimentology 44, 893–914.

Folk, R.L., Chafetz, H.S., 2000. Bacterially induced microscale and nanoscale carbonate precipitates. In: Riding, R., Awramik, S.M. (Eds.), Microbial Sediments. Springer-Verlag, Berlin, Germany, pp. 40–49.

Franseen, E.K., Esteban, M., Ward, W.C., Rouchy, J., 1996. Models for Carbonate Stratigraphy from Miocene Reef Complexes of Mediterranean Region, vol. 5. SEPM Concept. Sedimentol. Paleontol, 384 p.

Frasier, M.L., Corsetti, F.A., 2003. Neoproterozoic carbonate shrubs. Interplay of microbial activity and unusual environmental conditions. Palaios 18, 378–387.

Görgen, S., Benzerara, K., Skouri-Panet, F., Gugger, M., Chauvat, F., Cassier-Chauvat, C., 2021. The diversity of molecular mechanisms of carbonate biomineralization by bacteria. Discov. Mater. 1, 1–20.

Guido, A., Jacob, J., Gautret, P., Laggoun-Defarge, F., Mastandrea, A., Russo, F., 2007. Molecular fossils and other organic markers as palaeoenvironmental indicators of the Messinian Calcare di Base Formation: normal versus stressed marine deposition (Rossano Basin, northern Calabria, Italy). Palaeogeogr. Palaeoclimatol. Palaeoecol. 255, 265–283.

Guido, A., Mastandrea, A., Demasi, F., Tosti, F., Russo, F., 2012. Organic matter remains in the laminated microfabrics of the Kess-Kess mounds (Hamar Laghdad, Lower Devonian, Morocco). Sediment. Geol. 263-264, 194–201.

Guido, A., Gerovasileiou, V., Russo, F., Rosso, A., Sanfilippo, R., Voultsiadou, E., Mastandrea, A., 2019. Composition and biostratinomy of sponge-rich biogenic crusts in submarine caves (Aegean Sea, Eastern Mediterrenean). Palaeogeogr. Palaeoclimatol. Palaeoecol. 534, 109338.

Guido, A., Sposato, M., Palladino, G., Vescogni, A., Miriello, D., 2022a. Biomineralization of primary carbonate cements: a new biosignature in the fossil record from the Anisian of Southern Italy. Lethaia 55, 1–21.

Guido, A., Rosso, A., Sanfilippo, R., Miriello, D., Belmonte, G., 2022b. Skeletal *vs* microbialite geobiological role in bioconstructions of confined marine environments. Palaeogeogr. Palaeoclimatol. Palaeoecol. 593, 110920.

Guido, A., Calcagnile, M., Talà, A., Tredici, S.M., Belmonte, G., Alifano, P., 2024. Microbial consortium involved in ferromanganese and francolite biomineralization in an anchialine environment (Zinzulùsa Cave, Castro, Italy). Sci. Total Environ. 936, 173423.

Heindel, K., Birgel, D., Peckmann, J., Kuhnert, H., Westphal, H., 2010. Formation of deglacial microbialites in coral reefs off Tahiti (IODP 310) involving sulfate reducing bacteria. Palaios 25, 618–635.

Hendry, J.P., Pearson, M.J., Trewin, N.H., Fallicks, A.E., 2006. Jurassic septarian concretions from NW Scotland record interdependent bacterial, physical and chemical processes of marine mudrock diagenesis. Sedimentology 53, 537–565.

Horodyski, R.J., Bloeser, V., Von der Haar, S., 1977. Laminated algal mats from a coastal lagoon, Laguna Mormona, Baja California. J. Sediment. Petrol. 47, 680–696.

Howell, J., Woo, J., Chough, S.K., 2011. Dendroid morphology and growth patterns: 3-D computed tomographic reconstruction. Palaeogeogr. Palaeoclimatol. Palaeoecol. 299, 335–347.

Ibarra, Y., Corsetti, F.A., Greene, S.E., Bottjer, D.J., 2014. Microfacies of the Cotham Marble: a tubestone carbonate microbialite from the Upper Triassic, Southwestern U. K. Palaios 29, 1–15.

Javor, B.J., Castenholz, R.W., 1981. Laminated microbial mats, Laguna Guerrero Negro, Mexico. Geomicrobiol J. 2, 237–273.

Kazmierczak, J., Coleman, M.L., Gruszczynski, M., Kempe, S., 1996. Cyanobacterial key to the genesis of micritic and peloidal limestones in ancient seas. Acta Palaeontol. Pol. 41, 319–338.

Kershaw, S., Li, Y., Crasquin-Soleau, S., Feng, Q., Mu, X., Collin, P.Y., Reynolds, A., Guo, L., 2007. Earliest Triassic microbialites in the South China block and other areas: controls on their growth and distribution. Facies 53, 409–425.
Kershaw, S., Crasquin, S., Li, Y., Collin, P.Y., Forel, M.B., Mu, X., Baud, A., Wang, Y., Xie, S., Maurer, F., Guo, L., 2012. Microbialites and global environmental change across the Permian–Triassic boundary: a synthesis. Geobiology 10, 25–47.
Krijgsman, W., Fortuin, A.R., Hilgen, F.J., Sierro, F.J., 2001. Astrochronology for the Messinian Sorbas Basin (SE Spain) and orbital (precessional) forcing for evaporite cyclicity. Sediment. Geol. 140, 43–60.
Lee, J.H., Riding, R., 2023. Stromatolite-rimmed thrombolite columns and domes constructed by microstromatolites, calcimicrobes and sponges in late Cambrian biostromes, Texas, USA. Sedimentology 70, 293–334.
Lee, J.H., Chen, J., Chough, S.K., 2015. The middle–late Cambrian reef transition and related geological events: a review and new view. Earth Sci. Rev. 145, 66–84.
Lencina, A.I., Soria, M.N., Gomez, F.J., Gérard, E., Farias, M.E., 2021. Composite microbialites: thrombolite, dendrolite, and stromatolite associations in a modern environment, Pozo Bravo lake, Salar de Antofalla, Catamarca Puna, Argentina. J. Sediment. Res. 91 (12), 1305–1330.
Martin, J.M., Braga, J.C., Riding, R., 1993. Siliciclastic stromatolites and thrombolites, late Miocene, S.E. Spain. J. Sediment. Petrol. 63, 131–139.
Milli, S., Tancredi, S., Margiotta, S., Tentori, D., 2024. The orogenic effects on forebulge evolution: a case study from Cenozoic deposits in the Salento Peninsula, Italy. Mar. Pet. Geol. 161, 106698.
Moissette, P., Saint Martin, J.P., André, J.P., Pestrea, S., 2002. L'association microbialite-bryozoaires dans le Messinien de Sicile et de Sardaigne. In: Néraudeau, D., Goubert, E. (Eds.), l'Événement messinien: approches paléobiologiques et paléoécologiques. Geodiversitas 24 (3), 611–623.
Moissette, P., Cornée, J.J., Mannaï-Tayech, B., Rabhi, M., André, J.P., Koskeridou, E., Méon, E., 2010. The western edge of the Mediterranean Pelagian Platform: a Messinian mixed siliciclastic–carbonate ramp in northern Tunisia. Palaeogeogr. Palaeoclimatol. Palaeoecol. 285, 85–103.
Monty, C.L.V., 1972. Recent algal stromatolitic deposits, Andros Island, Bahamas. Preliminary report. Geol. Rundsch. 61, 742–783.
Monty, C.L.V., 1976. The origin and development of cryptalgal fabrics. In: Walter, M.R. (Ed.), Stromatolites, Development in Sedimentology, 20. Elsevier, Amsterdam, pp. 193–249.
Neuweiler, F., Rutsch, M., Geipel, G., Reimer, A., Heise, K.H., 2000. Soluble humic substances from in situ precipitated microcrystalline calcium carbonate, internal sediment, and spar cement in a cretaceous carbonate mud-mound. Geology 28, 851–854.
Neuweiler, F., D'Orazio, V., Immenhauser, A., Geipel, G., Heise, K.H., Cocozza, C., Miano, T.M., 2003. Fulvic-acid-like organic compounds control nucleation of marine calcite under suboxic conditions. Geology 31, 681–684.
Neuweiler, F., Kershaw, S., Boulvain, F., Matysik, M., Sendino, C., McMenamin, M., Munnecke, A., 2023. Keratose sponges in ancient carbonates. A problem of interpretation. Sedimentology 70, 927–969.
Noffke, N., 2010. Geobiology: Microbial Mats in Sandy Deposits from the Archean Era to Today. Springer, Heidelberg, p. 193.
Pedley, H.M., 1978. A new lithostratigraphical and palaeoenvironmental interpretation for the coralline limestone formations (Miocene) of the Maltese Islands. Overseas Geol. Miner. Resour. 54, 1–17.
Pedley, H.M., 1979. Miocene bioherms and associated structures in the Upper Coralline limestone of the Maltese Islands: their lithification and palaeoenvironment. Sedimentology 26, 577–591.
Pope, M.C., Grotzinger, J.P., 2000. Controls on fabric development and morphology of tufas and stromatolites, Uppermost Pethei Group (1.8 Ga), Great Slave Lake, Northwest Canada. In: Grotzinger, J.P., James, N.P. (Eds.), Carbonate Sedimentation and Diagenesis in the Evolving Precambrian World. Special SEPM Publication 67, Tulsa, U.S.A, pp. 103–121.
Pratt, B.R., 1995. The origin, biota and evolution of deep-water mud mounds. In: Monty, C.L.V., Bosence, D.W.J., Bridges, P.H., Pratt, B.R. (Eds.), Carbonate Mud-Mounds. Their Origin and Evolution. IAS Special Publication 23, Blackwell, Oxford, pp. 49–123.
Reid, R.P., Visscher, P.T., Decho, A.W., Stolz, J.F., Bebout, B.M., Dupraz, C., MacIntyre, I. G., Paerl, H.W., Pinckney, J.L., Prufert-Bebout, L., Steppe, T.F., DesMarais, J., 2000. The role of microbes in accretion, lamination and early lithification of modern marine stromatolites. Nature 406, 989–992.
Reid, R.P., Dupraz, C., Visscher, P.T., Sumner, D.Y., 2003. Microbial processes forming marine stromatolites: microbe-mineral interactions with a three-billion year rock record. In: Krumbein, W.E., Paterson, D.M., Zavarzin, G.A. (Eds.), Fossil and Recent Biofilms: A Natural History of Life on Earth. Kluwer Academic Publications, Dordrecht, Netherlands, pp. 103–118.
Reitner, J., 1993. Modern cryptic microbialite/metazoan facies from Lizard Island (Great Barrier Reef, Australia): formation and concepts. Facies 29, 3–40.
Reitner, J., Neuweiler, F., 1995. Mud mounds: a polygenetic spectrum of fine-grained carbonate buildups. Facies 32, 1–69.
Reitner, J., Thiel, V., Zankl, H., Michaelis, W., Wörheide, G., Gautret, P., 2000. Organic and biogeochemical patterns in cryptic microbialites. In: Riding, R., Awramik, S.M. (Eds.), Microbial Sediments. Springer, Berlin, pp. 149–160.
Ricchetti, G., Ciaranfi, N., 2013. Note illustrative della Carta Geologica d'Italia alla scala 1:50.000 – foglio 537 Capo Santa Maria di Leuca. ISPRA – Servizio Geologico d'Italia, Litografia Artistica Cartografica, Firenze, p. 121.
Riding, R., 1988. Classification of microbial carbonates. 6th International Coral Reef Symposium, Benthic Microbes and Reefs, Discussion Section, Abstracts, Townsville, Australia, p. 5.
Riding, R., 1991. Classification of microbial carbonates. In: Riding, R. (Ed.), Calcareous Algae and Stromatolites. Springer-Verlag, Berlin, pp. 21–51.
Riding, R., 2000. Microbial carbonates: the geological record of calcified bacterial-algal mats and biofilms. Sedimentology 47, 179–214.
Riding, R., 2008. Abiogenic, microbial and hybrid authigenic carbonate crusts: components of Precambrian stromatolites. Geol. Croat. 61, 73–103.
Riding, R., Tomás, S., 2006. Stromatolite reef crusts, early cretaceous, Spain: bacterial origin of in situ-precipitated peloid microspar? Sedimentology 53, 23–34.
Riding, R., Virgone, A., 2020. Hybrid carbonates; in situ abiotic, microbial and skeletal co-precipitates. Earth Sci. Rev. 208, 103300.
Riding, R., Braga, J.C., Martin, J.M., 1991. Oolite stromatolites and thrombolites, Miocene, Spain: analogue of recent giant Bahamian examples. Sediment. Geol. 71, 121–127.
Roep, T.B., Beets, D.J., Dronkert, H., Pagnier, H., 1979. A prograding coastal sequence of wave-built structures of Messinian age, Sorbas, Almeria, Spain. Sediment. Geol. 22, 135–163.
Roep, T.B., Dabrio, C.J., Fortuin, A.R., Polo, M.D., 1998. Late highstand patterns of shifting and stepping coastal barriers and washover-fans (late Messinian, Sorbas Basin, SE Spain). Sediment. Geol. 116, 27–56.
Roveri, M., Flecker, R., Krijgsman, W., Lofi, J., Lugli, S., Manzi, V., Sierro, F.J., Bertini, A., Camerlenghi, A., De Lange, G.J., Govers, R., Hilgen, F.J., Hubscher, C., Meijer, P.T., Stoica, M., 2014. The Messinian Salinity Crisis: past and future of a great challenge for marine sciences. Mar. Geol. 349, 113–125.
Rowland, S.M., Shapiro, R.S., 2002. Reef patterns and environmental influences in the Cambrian and earliest Ordovician. In: Kiessling, W., Flügel, E., Golonka, J. (Eds.), Phanerozoic Reef Patterns. SEPM Special Publication 72, Tulsa, U.S.A, pp. 95–128.
Russo, F., Neri, C., Mastandrea, A., Baracca, A., 1997. The mud mound nature of the Cassian Platform Margins of the Dolomites, a case history: the Cipit boulders from Punta Grohmann (Sasso Piatto Massif, northern Italy). Facies 36, 25–36.
Saint Martin, J.P., 2001. Implications de la présence de mud-mounds microbiens au Messinien (Sicile, Italie). Earth Planet. Sci. 332, 527–534.
Saint Martin, J.P., André, J.P., 1992. Les constructions coralliennes de la plate-forme carbonatée messinienne de Malte. Géol. Méd. 19 (3), 145–163.
Saint Martin, J.P., Conesa, G., Cornée, J.J., 1996. A new type of Messinian composite microbialitic build-up (Salemi, Sicily, Italy). Sediment. Geol. 106, 51–63.
Saint Martin, J.P., André, J.P., Muller, J., Lapointe, P., 1997. Géométrie de la plate-forme carbonatée d'âge Messinien de Malte: mise en évidence de l'élévation du plan d'eau méditerranéen au cours du Messinien. CR Acad. Sci. Paris 324 (IIa), 729–736.
Saint Martin, J.P., Hlel, S., Debrie, J., Ben Moktar, N., Saint Martin, S., Mannai-Yaiech, B., 2023. Microbial influence in the Messinian sedimentation: example of Cap Bon (NE Tunisia). An. Paléont. 109, 102600.
Sami, T.T., James, N.P., 1996. Synsedimentary cements as Paleoproterozoic platform building blocks, Pethei Group, Northwestern Canada. J. Sediment. Res. 66, 209–222.
Sanz-Montero, M.E., Rodríguez-Aranda, J.P., García Del Cura, M.A., 2009. Bioinduced precipitation of barite and celestite in dolomite microbialites. Examples from Miocene lacustrine sequences in the Madrid and Duero Basins, Spain. Sediment. Geol. 222, 138–148.
Shapiro, R.S., Rigby, J.K., 2004. First occurrence of an in situ anthaspidellid sponge in a dendrolite mound (Upper Cambrian; Great Basin, USA). J. Paleontol. 78, 645–650.
Shapiro, R.S., Wilmeth, D.T., 2020. Part B, volume 1, chapter 8: microbialites. In: Treatise Online, vol. 134, pp. 1–24.
Suosaari, E.P., Stanley, M., Awramik, S.M., Reid, R.P., Stolz, J.F., Grey, K., 2018. Living dendrolitic microbial mats in Hamelin Pool, Shark Bay, Western Australia. Geosciences 8, 212.
Trichet, J., Défarge, C., 1995. Non-biologically supported organomineralization. Bull. Inst. Océan. 14, 203–236.
Usui, A., Hino, H., Suzushima, D., Tomioka, N., Suzuki, Y., Sunamura, M., Kato, S., Kashiwabara, T., Kikuchi, S., Uramoto, G.I., Suzuki, K., Yamaoka, K., 2020. Modern precipitation of hydrogenetic ferromanganese minerals during on-site 15-year exposure tests. Sci. Rep. 10, 3558.
Vescogni, A., Bosellini, F.R., Reuter, M., Brachert, T.C., 2008a. Vermetid reefs and their use as palaeobathymetric markers: new insights from the Late Miocene of the Mediterranean (Southern Italy, Crete). Palaeogeogr. Palaeoclimatol. Palaeoecol. 267, 89–101.
Vescogni, A., Guido, A., Russo, F., 2008b. Vermedits-microbialites association: an example of peculiar carbonate production from the late Miocene of the Salento Peninsula. Rend. Online Soc. Geol. It. 2, 187–189.
Vescogni, A., Guido, A., Mastandrea, A., Russo, F., 2011. Microbialite-vermetid community (Salento Peninsula, southern Italy): a late Miocene example of automicrite deposition. In: Reitner, J., Quéric, N.V., Arp, G. (Eds.), Advances in Stromatolite Geobiology, Lect. Notes Earth Sci, vol. 131, pp. 321–329.
Vescogni, A., Vertino, A., Bosellini, F.R., Harzhauser, M., Mandic, O., 2018. New paleoenvironmental insights on the Miocene condensed phosphatic layer of Salento (southern Italy) unlocked by the coral-mollusc fossil archive. Facies 64, 7.
Vescogni, A., Guido, A., Cipriani, A., Gennari, R., Lugli, F., Lugli, S., Manzi, V., Reghizzi, M., Roveri, M., 2022. Palaeoenvironmental setting and depositional model of upper Messinian microbialites of the Salento Peninsula (Southern Italy): a central Mediterranean Terminal Carbonate Complex. Palaeogeogr. Palaeoclimatol. Palaeoecol. 595, 110970.
Vescogni, A., Colombo, F., Guido, A., 2025. New insights into upper Messinian microbial carbonates: a dendrolite-thrombolite build-up from the Salento Peninsula, central Mediterranean. Geobiology 23, e70023.

Woo, J., Chough, S.K., Han, Z., 2008. Chambers of *Epiphyton thalli* in microbial buildups, Zhangxia formation (middle Cambrian), Shandong Province, China. Palaios 23, 55–64.
Wu, S., Chen, Z.Q., Fang, Y., Pei, Y., Yang, H., Ogg, J., 2017. A Permian-Triassic boundary microbialite deposit from the eastern Yangtze Platform (Jiangxi Province, South China): geobiologic features, ecosystem composition and redox conditions. Palaeogeogr. Palaeoclimatol. Palaeoecol. 486, 58–73.
Zhang, Y., Hoffmann, L., 1992. Blue-green algal mats of the salinas in San-ya, Hai-nan Island (China): structure, taxonomic composition, and implications for the interpretation of Precambrian stromatolites. Precambrian Res. 56, 275–290.